LONDON, METEOROLOGICAL OFFICE.

Met.O.15 Internal Report No.44.

An introduction to the numerical study of frontal zones. By BENNETTS,D.A.

London,Met.Off.,Met.O.15 Intern.Rep.No.44, 1982,Pp.42.21 Refs.

An unofficial document - not to be quoted in print.

METEOROLOGICAL OFFICE
London Road, Bracknell, Berks.

MET.O.15 INTERNAL REPORT

No 44

AN INTRODUCTION TO THE NUMERICAL STUDY OF FRONTAL ZONES

by

D A Bennetts

April 1982

Cloud Physics Branch (Met.O.15)

FRONTAL SYSTEMS 1.

1. INTRODUCTION

Frontal systems are an important part of the climatology of the United Kingdom and contribute significantly to the total annual rainfall. A front delineates the boundary between two different air masses. The position of the boundary is determined by the motion of the larger scale cyclones and anticyclones but the structure of the boundary is determined by the local mesoscale processes, ie on a scale of 10–100 km. This is illustrated by the fact that global forecast models predict only the gross features of a front and it is left to the forecaster to predict the finer details. The way to improve the forecasting of fronts is to understand the mesoscale structure and to try and relate it to the larger synoptic scale motion.

2. OBSERVATIONS

There are three principal means of making observations of frontal systems. The first is by releasing radiosondes at frequent intervals as the front passes over the radiosonde station. This allows a cross section to be obtained but suffers from the disadvantage that the observations span some 6–12 hours during which time there may be substantial development on either the synoptic or the mesoscale, frequently both. The value of the observations is increased by using more than one radiosonde station but there remains a fundamental difficulty, namely the measurements must be made over land. Orographic effects are inextricably mixed with frontal motions. That does not invalidate the experiment but it does make the interpretation of the data much more difficult.

The second method of making observations is by instrumented aircraft. The speed of the aircraft enables horizontal passes to be made on a time scale short compared with the development of the system but whereas the restriction with radiosondes was the horizontal coherence of vertical profiles, here the problem is the vertical coherence of horizontal passes.

The third method, developed by the office, involves releasing dropsondes from an aircraft as it flies above a front. Five of these can be tracked simultaneously and the aircraft can therefore fly across a front dropping a sonde every 20 or 30 km. A complete cross-section can therefore be built up in under an hour, which is in effect a snapshot of the structure of the front.

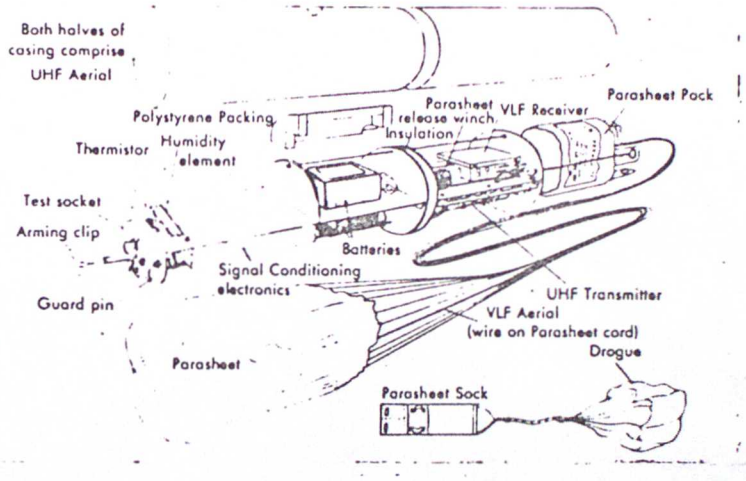

Figure 1. The Meteorological Office wind-finding dropsonde.

Figure 1 shows a cut away section of a dropsonde. Contained within the body of the sonde, but exposed to the free flow of air, is a pressure sensor, accurate to $\pm$ 2 mb, a humidity element, accurate to $\pm$ 5%, and a temperature sensor accurate to $\pm$ 0.2°C. The sonde is suspended beneath a parachute designed specifically for its wind following characteristics. The winds are ascertained to $\pm$ 0.5 ms^{-1} by recording the position of the sonde every second. This is achieved by using the LORAN C navigation system which covers most of the North Atlantic. A master and two slave

stations send out radio signals at a fixed interval of time apart. By measuring the change in this interval at the receiving station it is possible to accurately measure the sonde's position. The resultant accuracy in wind speed is shown in Figure 2 for various combinations of master and slave stations.

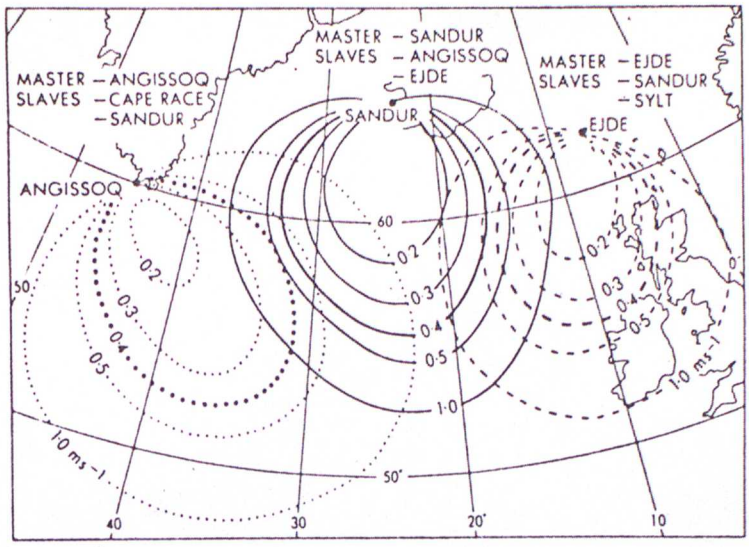

Figure 2. Predicted RMS 1 minute wind errors for daytime using the indicated Loran C transmitters.

3. STRUCTURE OF A WARM FRONT

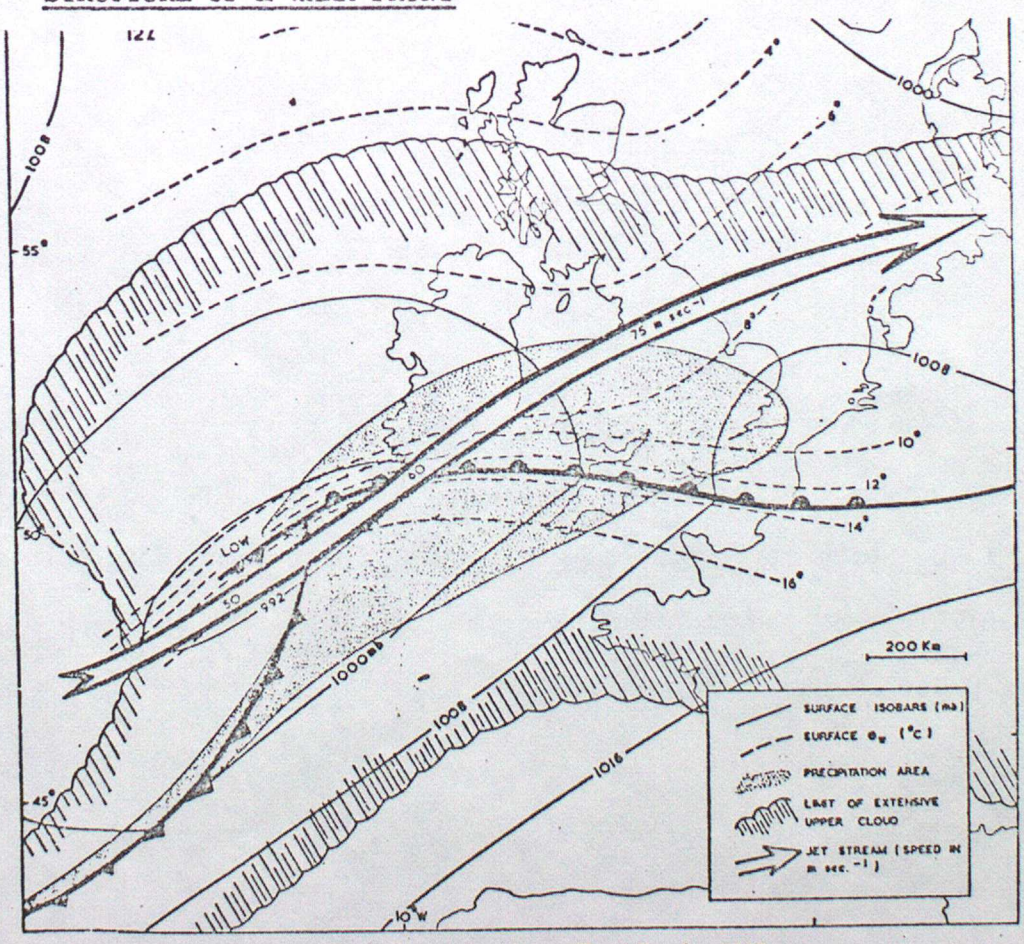

Figure 3. Synoptic situation 12 Z, 16 October 1967.

Figure 3 depicts a classic wave depression approaching the United Kingdom. The cloud canopy and precipitation areas are shown in relation to the surface warm and cold fronts but for a deeper understanding it is necessary to look at the vertical structure.

Figure 4 shows the synoptic situation at midday on 29 March 1979, the time at which several sondes were dropped on an East-West line at $\sim 55^{\circ}$N through warm front 'S'.

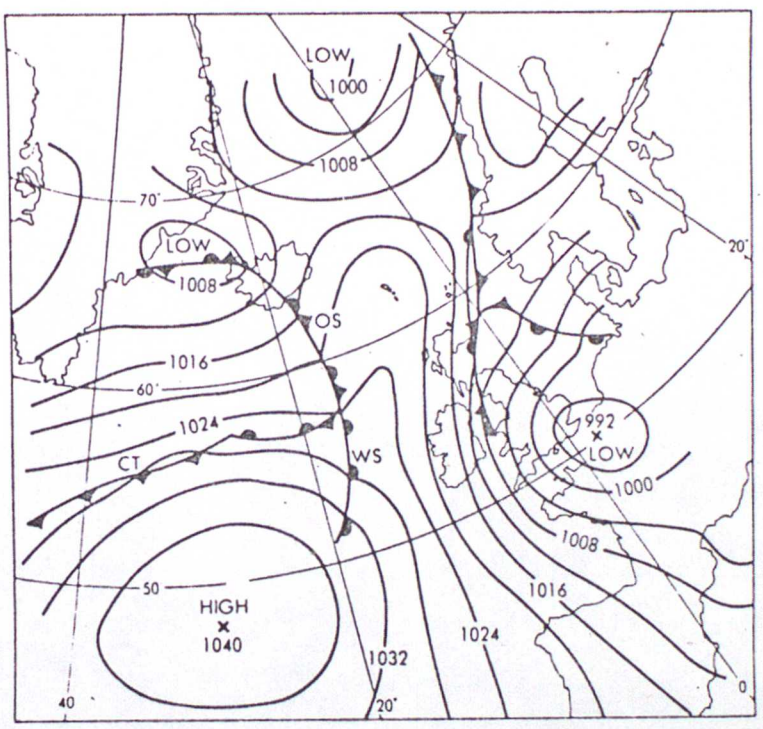

Figure 4. Surface analysis for 1200 GMT 29 March 1979.

It is convenient to present the data in a (p , x - st) frame of reference where p is the pressure and s (12.5 ms^{-1}) the component of the system velocity vector in the x direction, West to East in this case. The origin of the x co-ordinate is arbitrarily set to the West of the most upstream observation.

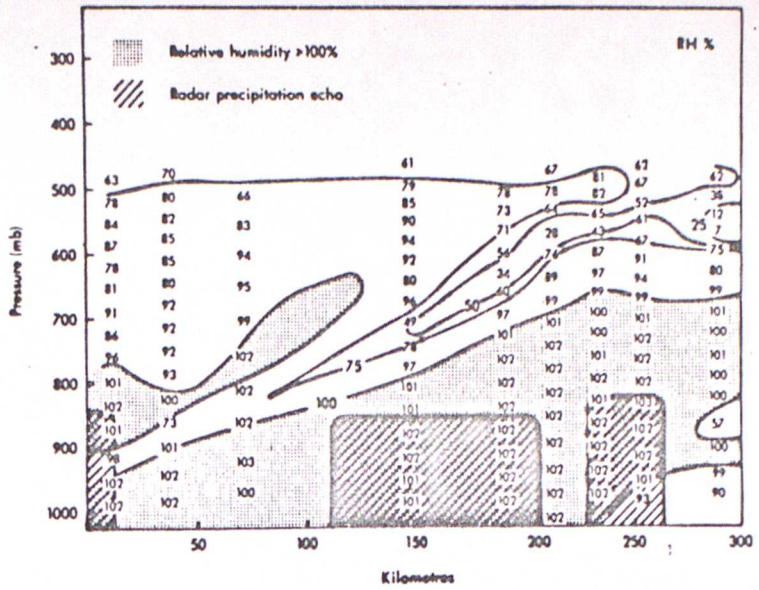

Figure 5. East-West cross section of relative humidity and radar echo.

Figure 5 shows the variation of relative humidity in this frame of reference. The major feature is the layer of saturated air in the lower half of the figure with a long sloping tongue of dry air overlaying it. Above the dry zone the air is moist again. The location of the radar echo, ie regions of precipitation, is superimposed on the diagram. I_n this example the precipitation is banded, a common feature of front but by no means universal. The same is true of the dry tongue of air above the frontal surface.

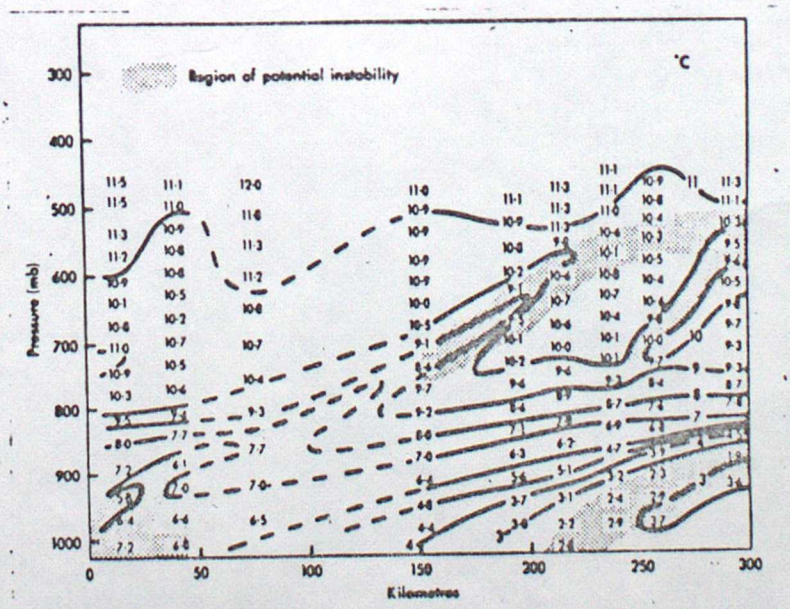

Figure 6. East-West cross section of wet bulb potential temperature.

The field of wet bulb potential temperature, Figure 6, exhibits the expected strong gradient at the frontal zone extending from the surface, at 150 km, to 850 mb at 300 km. Of special interest are the hatched regions denoting air which is potentially unstable. The two zones below 900 mb are saturated and represent regions where the measured lapse rate is at or greater than the moist adiabatic indicated that convection could take place. The band of potential unstable air above the frontal surface corresponds to the dry tongue of air identified in Figure 5; being so dry it is unlikely that this potential instability will be released.

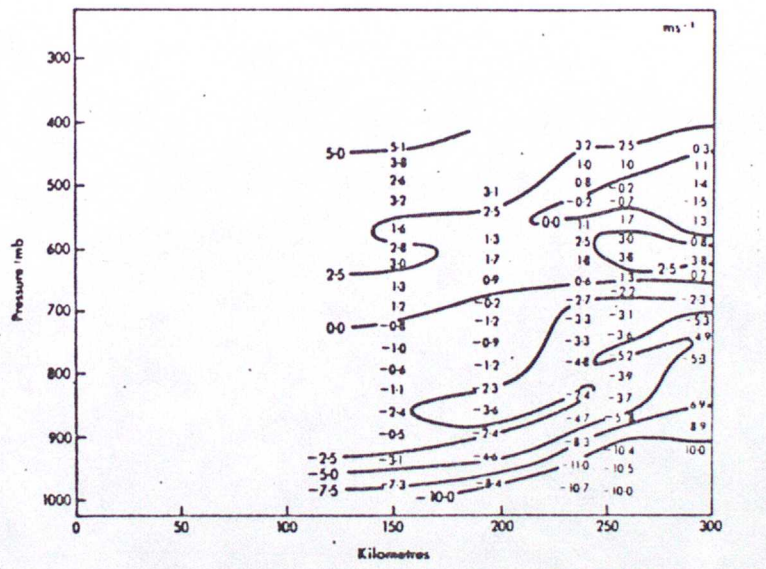

Figure 7. East-West cross section of westerly component of wind relative to the system, assumed to be moving at $270^{o}/12.5$ ms^{-1}.

Figure 7 shows the u-component of velocity relative to the system. As expected air above the front is moving to the East and over-running that beneath the front.

4. THEORY

There are many features in the above observations that require detailed analysis. However before embarking on this it is important to review the theory of frontal motions.

There are four basic regimes of modelling:-

a. Geostrophic

Geostrophic theory is simple and well understood. It is useful for short range forecasting - for example ascertaining the wind speed from the surface isobars - and estimating orders of magnitude.

b. Quasi-Geostrophic

This is the name given to the analysis of small perturbations of a steady geostrophic flow. The magnitude of the perturbation is given by the Rossby number, defined U/fL where U is a characteristic velocity, f the coriolis parameter and L a length scale. Quasi-geostrophic theory is widely used as over a wide range of problems and scales the Rossby number is small. Additionally, even if R is not small ie $0.1 \lesssim R \lesssim 1$, the results of the theory are qualitatively useful.

c. Quasi-Geostrophic +

This is an extension of the above theory and represents the approach outlined in the Cumulonimbus lectures. It involves looking carefully at the problem and selecting just those extra terms that both give insight into the problem and are consistent within the frame work of the equations.

d. Full Navier-Stokes equation

The final alternative is to use the full equations of motion. This has the merit that once the model is formulated and developed it can be applied to a wide range of problems. However it suffers from exactly the same fact. It is difficult to isolate the cause of any given behaviour. In addition it is more complex than required for any specific problem.

To understand these various approximations consider the full equations of motion

$$\left.\begin{aligned} \frac{Du}{Dt} - fv &= -\frac{1}{\rho}\frac{\partial p}{\partial x} \\ \frac{Dv}{Dt} + fu &= -\frac{1}{\rho}\frac{\partial p}{\partial y} \end{aligned}\right\}$$ horizontal momentum

$$\frac{Dw}{Dt} + g = -\frac{1}{\rho}\frac{\partial p}{\partial z}$$ vertical momentum

$$\frac{D\rho}{Dt} + \rho\, \mathrm{div}(u,v,w) = 0$$ continuity

$$\frac{D\theta}{Dt} = 0$$ conservation of potential temperature

$$\left.\begin{aligned} p &= RT\rho \\ T &\propto \theta p^{0.286} \end{aligned}\right\}$$ equations of state.

Although the (x,y,z) co-ordinate system is the easiest to understand, the atmosphere does not recognise height as a meaningful variable; pressure is a more natural vertical ordinate. However, as was found in the discussion of cumulonimbus convection, pressure also has its disadvantages. A good compromise is to use a pseudo height z' defined as

$$z' = \left(\frac{R\theta_0}{gk}\right)\left(1 - p/p_0\right)^k ; \qquad k = R/c_p$$

and θ_0 and p_0 are standard values.

In an adiabatic atmosphere z' and h are identical but in a normal mid-latitude atmosphere p = 300 mb is equivalent to z' = 8000 and h = 9200 m. In consequence z' may be thought of as height but in addition has many of the attributes of pressure.

To simplify the following argument assume the hydrostatic and Boussinesq approximation, and define ϕ as the geopotential gz'.

The equations then become, relative to the co-ordinates (x, y, z'), (dropping the prime notation),

$$\frac{Du}{Dt} - fv + \frac{\partial \phi}{\partial x} = 0 \qquad (1)$$

$$\frac{Dv}{Dt} + fu + \frac{\partial \phi}{\partial y} = 0$$

$$\frac{D\theta}{Dt} = 0$$

$$\frac{\partial u}{\partial x} + \frac{\partial v}{\partial y} + \frac{\partial w}{\partial z} = 0$$

$$\frac{\partial \phi}{\partial z} = \left(\frac{g}{\theta_0}\right)\theta$$

Write

$$x = Lx', \quad y = Ly', \quad z = Hz', \quad t = Tt'$$

$$u = Uu', \quad v = Vv', \quad w = Ww', \quad \phi = LfV\phi', \quad \theta = \frac{LfV k \theta_0 \theta'}{g}$$

and substitute into equation (1) which, expanded, is

$$\frac{\partial u}{\partial t} + u\frac{\partial u}{\partial x} + v\frac{\partial u}{\partial y} + w\frac{\partial u}{\partial z} - fv + \frac{\partial \phi}{\partial x} = 0$$

and becomes

$$\frac{U}{T}\frac{\partial u}{\partial t} + \frac{U^2}{L}\frac{\partial u}{\partial x} + \frac{UV}{L}\frac{\partial u}{\partial y} + \frac{WU}{H}\frac{\partial u}{\partial z} - fVv + \frac{LfV}{L}\frac{\partial \phi}{\partial x} = 0$$

Define

$$R_t = \frac{1}{fT}, \quad R_x = \frac{U}{fL}, \quad R_y = \frac{V}{fL}, \quad R_z = \frac{W}{fH}$$

Then

$$\frac{D}{Dt} = R_t\frac{\partial}{\partial t} + R_x\frac{\partial}{\partial x} + R_y\frac{\partial}{\partial y} + R_z\frac{\partial}{\partial z}$$

and the equation can be written

$$\frac{U}{V}\frac{Du}{Dt} - v + \frac{\partial \phi}{\partial x} = 0.$$

The various R_i are called the Rossby numbers and their values depend on the atmospheric phenomena under consideration.

For simplicity let all the $R_i = R$ and $u=V$ and consider a perturbation about a mean state ie

$$u = u_g + Ru' \ldots$$
$$v = v_g + Rv' \ldots$$
$$w = Rw' \ldots$$
$$\theta = \theta_s + R\theta' \ldots$$
$$\phi = \phi_s + R\phi' \ldots$$

where θ_s and ϕ_s are the mean state of the basic atmosphere.

Substitute into the equations and collect together all terms of $O(R^0)$. This leads to the geostrophic equations of motion namely

$$-v_g + \frac{\partial \phi_s}{\partial x} = 0$$

$$u_g + \frac{\partial \phi_s}{\partial y} = 0$$

$$\frac{\partial \phi_s}{\partial z} - \theta_s = 0$$

$$\frac{\partial u_g}{\partial x} + \frac{\partial v_g}{\partial y} = 0$$

Making use of the observational fact that fronts appear two dimensional, the variation in y is neglected giving

$$u_g = 0$$

ie there is no flow across the frontal surface

and $$\frac{\partial v_g}{\partial z} = \frac{\partial \theta_s}{\partial x}$$

Now the slope of the isotherm is given by

$$\text{Tan}\,\psi = \frac{\partial\theta_s/\partial x}{\partial\theta_s/\partial z} = \left(\frac{dz}{dx}\right)_{\theta_s}$$

and in consequence the slope of the frontal surface is

$$\text{Tan}\,\psi = \frac{\partial v_g}{\partial z} \Big/ \frac{\partial\theta_s}{\partial z} = \frac{\delta v_g}{\delta\theta_s}$$

or

$$\text{Tan}\,\psi = \frac{(v_{g_W} - v_{g_C})}{(\theta_{s_W} - \theta_{s_C})} \qquad \text{(scaled variables).}$$

where the subscript W and C refer to the warm and cold air respectively. This is called the Margules solution (1890) and implies

1) There is no cross frontal circulation.

2) The frontal surface is a straight line.

3) The front is stationary with respect to the mean flow.

Clearly the Geostrophic equation of motion are insufficient to realistically represent a front.

Return to the equation of motion and collect together all terms $O(R^0 + R')$. The resulting equations are called <u>QUASI-GEOSTROPHIC</u>.

$$\frac{u}{v}\frac{Du_g}{Dt} - v + \frac{\partial\phi}{\partial x} = 0$$

$$\frac{v}{u}\frac{Dv_g}{Dt} + u + \frac{\partial\phi}{\partial y} = 0$$

$$-\theta + \frac{\partial\phi}{\partial z} = 0$$

$$\frac{\partial u}{\partial x} + \frac{\partial v}{\partial y} + \frac{\partial w}{\partial z} = 0$$

$$\frac{D\theta}{Dt} + w\frac{\partial\theta_s}{\partial z} = 0$$

$$\frac{D}{Dt} = \frac{\partial}{\partial t} + u_g\frac{\partial}{\partial x} + v_g\frac{\partial}{\partial y} = O(R)$$

$$u_g = -\frac{\partial\phi}{\partial y} \; ; \; v_g = \frac{\partial\phi}{\partial x}$$

Note especially the form of D/Dt, and that the full velocity occurs only in 'rotation' terms and in the continuity equation.

In frontal regions

$L \sim 50$ km $\quad L \sim 500$ km $\quad h \sim 8$ km

$U \sim 2\text{-}3$ m s^{-1} $\quad V \sim 20$ m s^{-1} $\quad W \sim 1$ m s^{-1}

In consequence

$$R_x \simeq R_{\gamma} \simeq R_z \simeq R_t = R$$

as already assumed

but

$$\frac{U}{V} << 1$$

implying that

$$V_g = \frac{\partial \phi}{\partial x}$$

ie motion in the cross-frontal direction is in geostrophic balance

and

$$\frac{DV_g}{Dt} + u + \frac{\partial \phi}{\partial y} = 0$$

ie motion in the long-front direction is quasi-geostrophic.

5. GENERATION OF A FRONT

Consider now the characteristics of a quasi-geostrophic front.

Firstly, what sort of atmospheric motion can generate strong gradients. Figure 8 shows four possible ways; horizontal deformation, horizontal shear, vertical deformation and vertical shear. Figure 9 illustrates where some of these might occur within cyclones and anti-cyclones.

If these deformation fields are put into a quasi-geostrophic model as initial conditions and the equation integrated a front, Figure 10, forms.

Horiz deformation

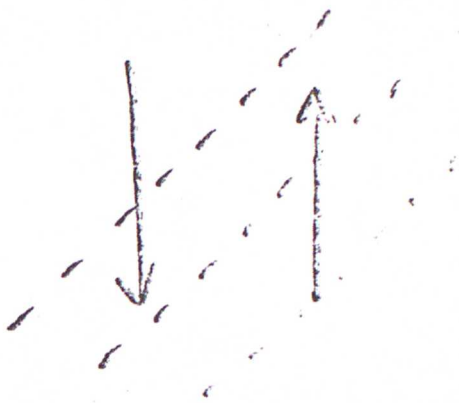

Horiz Shear

Vertical Deformation

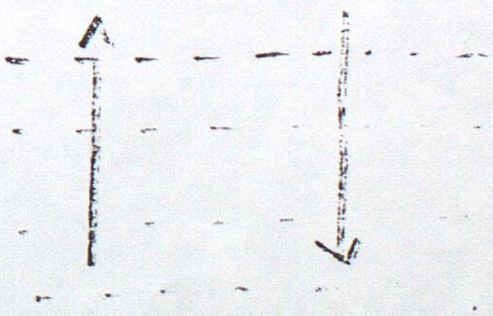

Vertical Shear

Figure 8. Deformation fields that can lead to frontogenesis.

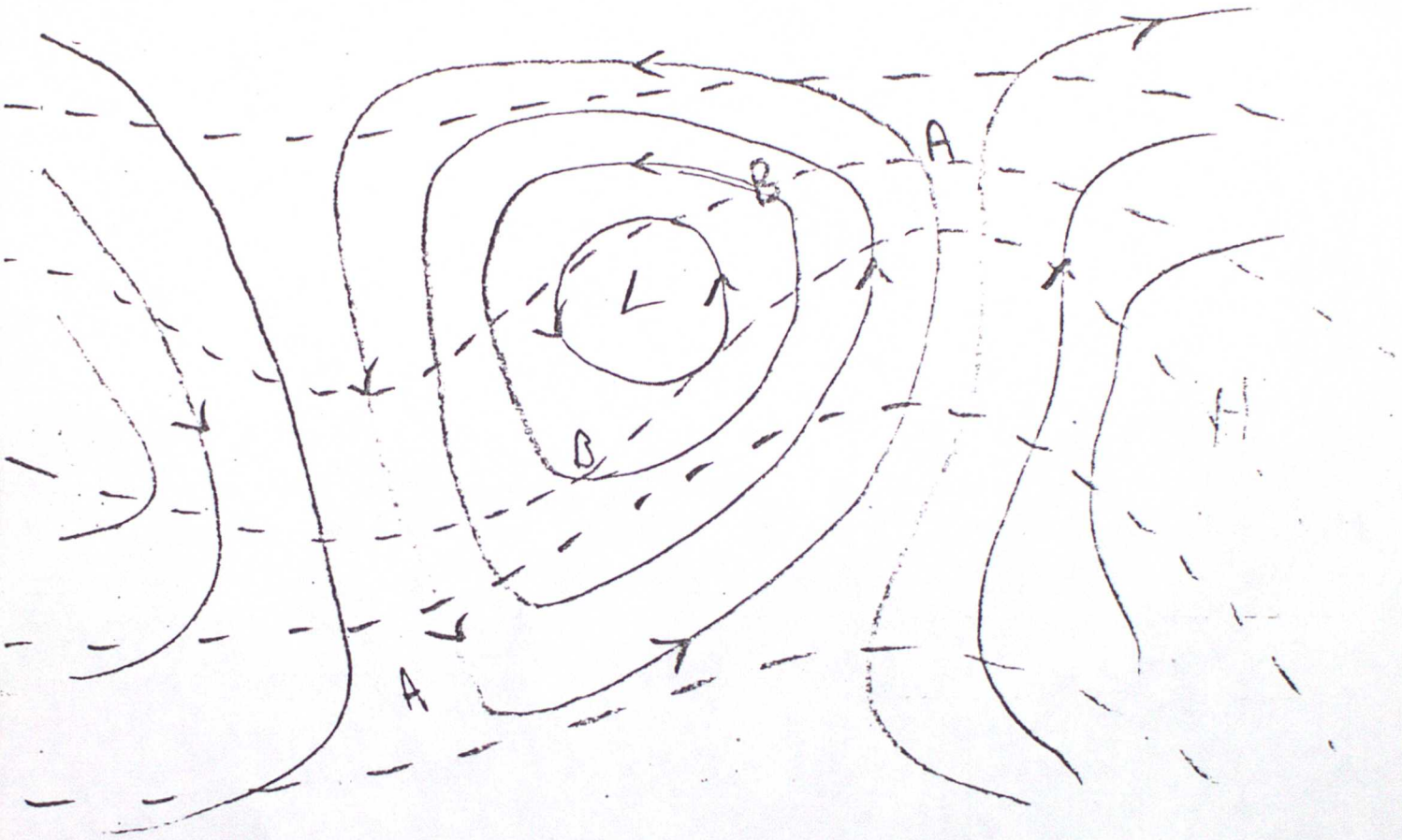

A – horizontal deformation

B – horizontal shear.

Figure 9. Regions within a cyclone favourable for the formation of frontal systems.

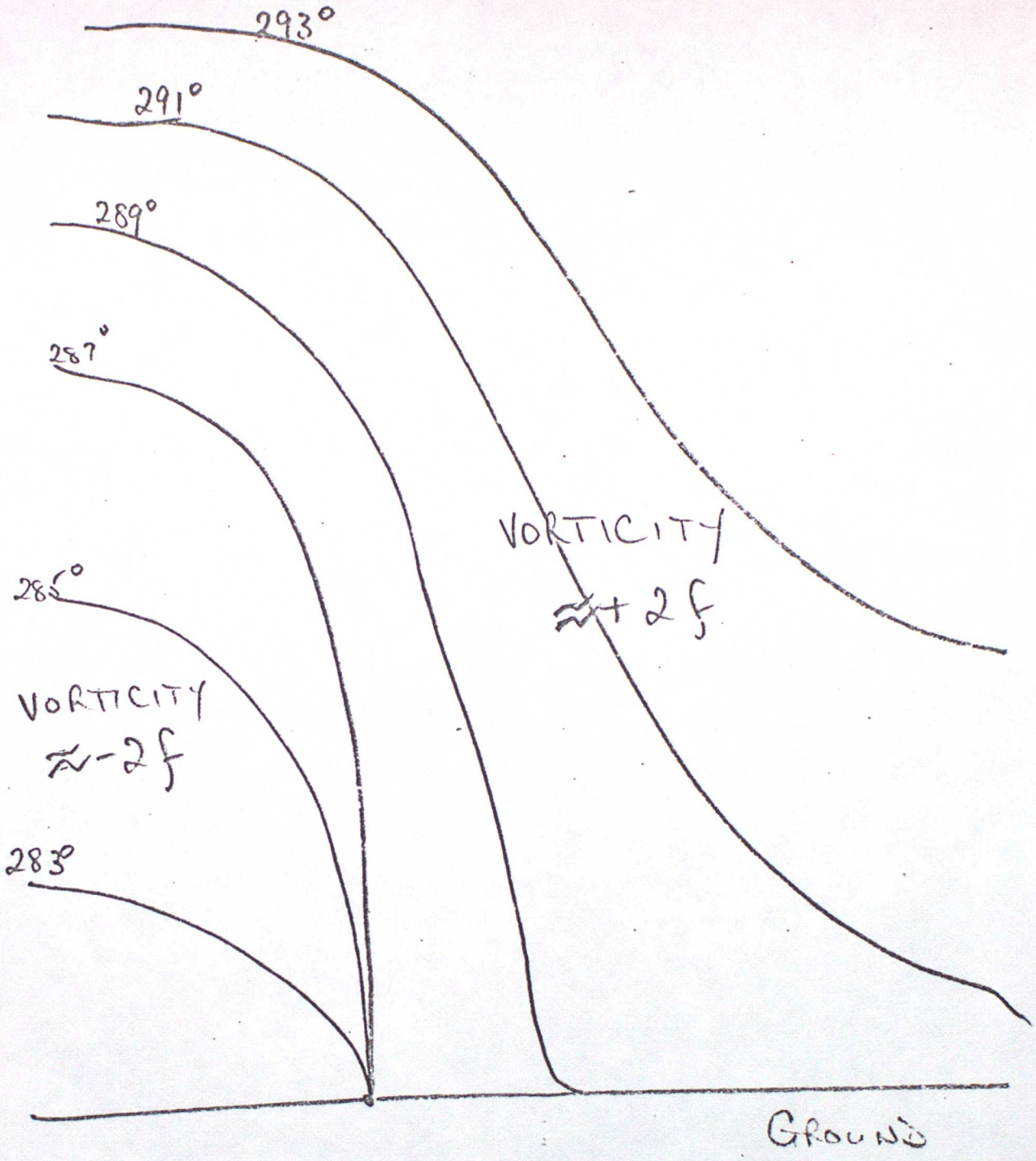

Figure 10. The field of potential temperature resulting from horizontal deformation. The field was generated by numerical integration of the QUASI-GEOSTROPHIC equations.

The isotherms form a discontinuity at the surface and the front becomes weaker with height, both features being in general accord with observations. As friction has been neglected from the model, the discontinuity eventually becomes infinite, but this does not detract from the general conclusions.

The unreality of the model only becomes apparent when the cross-frontal circulations are considered. These show that the vorticity $\left(\frac{\partial v}{\partial x}\right)$ rises * to $\pm 2f$. Such values are never observed and so, although the quasi-geostrophic approximation is an improvement it is still not entirely suitable for the study of frontal systems.

* i.e. $-f \leq f + \frac{\partial v}{\partial x} \leq 3f$.

Suggested reading.

*	Browning and Harrold	1969	Air motion and precipitation growth in a wave depression. QJRMS 95, p 288.
	Browning and others	1973	The structure of rain bands within a mid-latitude depression. QJRMS 99, p 215.
	Hoskins B J	1974	The role of potential vorticity in symmetric stability and instability. QJRMS 100, p 480.
	Roach and Hardman	1975	Mesoscale air motions derived from wind finding dropsonde dat : the warm front and rain bands of January 1971. QJRMS 101, p 437.
*	Hoskins and Bretherton	1972	Atmospheric Frontogenesis Models: Mathematical formulation and solution. JAS 29, p 11.
	Stone P M	1966	Frontogenesis by horizontal wind deformation fields. JAS 23, p 455.
	Pedlosky J	1964	The stability of Currents in the Atmosphere and the Ocean Part I. JAS 21, p 201.
	Williams and Plotkin	1968	Quasi-Geostrophic Frontogenesis. JAS 25, p 201.
	Hoskins	1975	The Geostrophic Momentum approximation and the Semi-Geostrophic Equations. JAS 32, p 233.
	Hoskins, Draghici, Davies	1978	A new look at the - equ. QJRMS 104, p 31.
*	Editor - Roberts & Howard	1978	Rotating fluids in Geophysics, pub. Academic Press.

1. INTRODUCTION

At the end of the last lecture it was demonstrated that the quasi-GEOSTROPHIC equations could produce a realistic 'thermodynamic' front but that the associated 'dynamical' variables were less than satisfactory. It will be recalled that the relevant equations were

2-D with $\frac{\partial \phi}{\partial y} = \frac{\partial \phi}{\partial y}(x,z)$ only

$$\frac{Dv_g}{Dt} + fu + \frac{\partial \phi}{\partial y} = 0$$

$$\frac{g\theta}{\theta_0} = \frac{\partial \phi}{\partial z}$$

$$\frac{D\theta}{Dt} + w\frac{\partial \theta_s}{\partial z} = 0$$

$$\frac{\partial u}{\partial x} + \frac{\partial w}{\partial z} = 0$$

with $u = u_g + u'$, $v = v_g + v'$

and $$\frac{D}{Dt} = \frac{\partial}{\partial t} + u_g \frac{\partial}{\partial x}$$

To understand why the quasi-geostrophic equations do not give realistic fronts it is necessary to examine them in detail.

Consider the θ - eqn.

Define the Brunt-Vaisala frequency $N^2 = \frac{g}{\theta_0}\frac{\partial \theta_s}{\partial z}$

then $$\frac{D\theta}{Dt} = -wN^2$$

Therefore

$$\frac{D}{Dt}\left(\frac{g}{\theta_0}\frac{\partial \theta}{\partial x}\right) = -N^2\frac{\partial w}{\partial x} - \frac{\partial u_g}{\partial x}\frac{g}{\theta_0}\frac{\partial \theta}{\partial x}$$

Define $S^2 = \frac{g}{\theta_0}\frac{\partial \theta_s}{\partial x}$ and, neglecting small terms

$$\frac{D}{Dt}\left(\frac{g}{\theta_0}\frac{\partial \theta}{\partial x}\right) = -N^2\frac{\partial w}{\partial x} - S^2\frac{\partial u_g}{\partial x}$$

Similarly from the horizontal momentum equation

$$\frac{D}{Dt}\left(f\frac{\partial v_g}{\partial z}\right) = -f^2\frac{\partial u}{\partial z} - f\frac{\partial u_g}{\partial z}\frac{\partial v_g}{\partial x}$$

But $f\frac{\partial v_g}{\partial z} = \frac{g}{\theta_0}\frac{\partial \theta}{\partial x}$ and hence

$$-N^2\frac{\partial w}{\partial x} - S^2\frac{\partial u_g}{\partial x} = -f^2\frac{\partial u}{\partial z} - f\frac{\partial u_g}{\partial z}\frac{\partial v_g}{\partial x}$$

or

$$f^2\frac{\partial u}{\partial z} - N^2\frac{\partial w}{\partial x} = \text{Constant (of basic flow)}.$$

Continuity implies $u = \frac{\partial \psi}{\partial z}$, $w = -\frac{\partial \psi}{\partial x}$

$$\therefore f^2 \frac{\partial^2 \psi}{\partial z^2} + N^2 \frac{\partial^2 \psi}{\partial x^2} = \text{Constant} \quad (1)$$

i.e. all motion takes place in elipses and hence is symmetric. It will be recalled that one of the problems of a quasi-geostrophic front was that the vorticity was -2f on one side and +2f on the other.

In the second lecture on Cumulonimbus convection a technique was described to isolate and identify small terms that were important to the development of convective motion. If the same technique is applied here a set of equations, usually referred to as the SEMI-GEOSTROPHIC equation, results.

$$\frac{Dv_g}{Dt} + fu + \frac{\partial \Phi}{\partial y} = 0$$

$$\theta \frac{g}{\theta_0} - \frac{\partial \Phi}{\partial x} = 0$$

$$\frac{\partial u}{\partial x} + \frac{\partial w}{\partial z} = 0$$

$$\frac{D\theta_s}{Dt} = 0$$

and

$$\frac{D}{Dt} = \frac{\partial}{\partial t} + u\frac{\partial}{\partial x} + w\frac{\partial}{\partial z}$$

The SEMI-GEOSTROPHIC equation differs from the QUASI-GEOSTROPHIC in one respect; advection takes place with the full velocity rather than the geostrophic velocity. It is a small but important difference as it allows upgliding of first order quantities.

Applying the same analysis technique as before leads to the equation

$$-N^2 \frac{\partial^2 \psi}{\partial x^2} + 2S^2 \frac{\partial^2 \psi}{\partial x \partial z} - F^2 \frac{\partial^2 \psi}{\partial z^2} = \text{const}$$

i.e. a cross-product term is introduced and f^2 replaced by $F^2 = f\left(f + \frac{\partial v_g}{\partial x}\right)$.

By making the transformation $X = x + \frac{v_g}{f}$ the equation becomes

$$f^2 \frac{\partial^2 \psi}{\partial z^2} + \frac{\partial}{\partial x}\left(q \frac{\partial \psi}{\partial x}\right) = \text{constant} \quad (2)$$

q, Ertels potential vorticity ($= N^2F^2 - S^4$) may be considered as a slight modification to N^2 and then it can be seen that the form of equation (1) and (2) are similar.

In consequence, solutions obtained for the quasi-GEOSTROPHIC front remain

valid for a SEMI-GEOSTROPHIC front except that the co-ordinate system is changed from (x,z) to (X,z). The effect of this is illustrated in Figure 1. Figure 1a shows a solution to the quasi-geostrophic equations in the form of a roll in the (x,z) plane. Such a circulation implies a motion in the y-direction (v), out of the paper at the bottom, and into the paper at the top, V is < 0 and > 0 respectively. Using the semi-geostrophic equations and transforming back to the (x,z) plane from the (X,z) plane, increases the horizontal separation at the top and decreases it at the bottom (Figure 1b).

Gradients become stronger where there is positive vorticity and weaker whenever the vorticity is less than f. The symmetry of the quasi-geostrophic front is destroyed and regions of strong negative absolute vorticity eliminated. In consequence a much better representation of a front is obtained.

In summary, there are three stages in the formation of a front.

a) Due to large scale motions there exists a basic deformation field. This flow may be represented by the geostrophic equations.

b) The deformation field modifies the temperature field which leads to the generation of small perturbations in the velocity field. While the motions are characterised by $\frac{\partial v}{\partial x} << f$ this stage of frontal development may be described by the quasi-geostrophic equations.

c) However as the velocities increase in magnitude, ie the size of becomes comparable with f, they act in such a way as to enhance the frontogenetic process. There is a positive feed-back and the stronger the front, the stronger are the forces maintaining it. This phase may be described by the semi-geostrophic equation.

2. INSTABILITIES ON FRONTS

Studies of the mesoscale organization of cyclones and their frontal systems have shown that almost everywhere the precipitation can, and frequently does, exhibit an organization on several scales. Viewed on horizontal maps the larger features, 50-100 km wide, are usually banded and orientated parallel to one of the fronts. These larger features typically contain smaller areas,

QUASI-GEOSTROPHIC

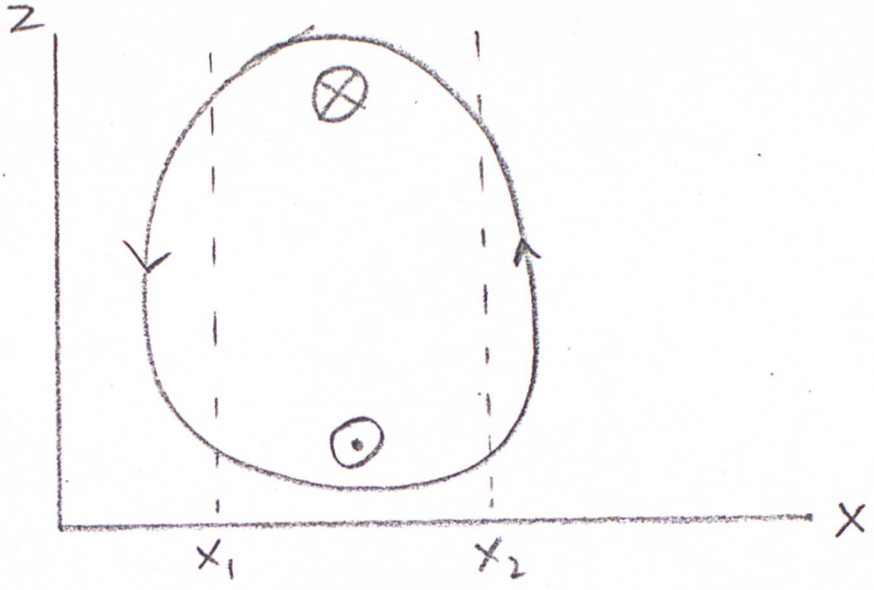

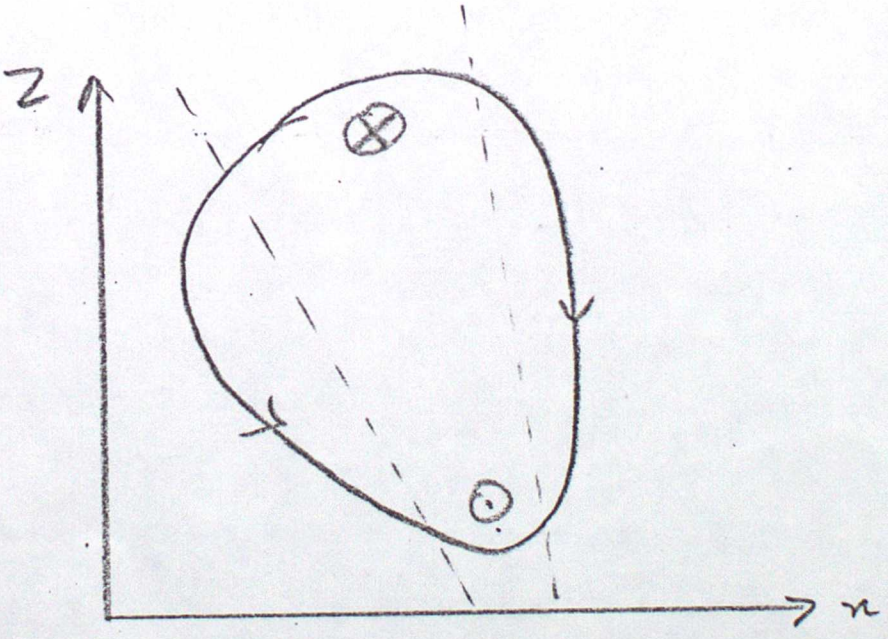

QUASI-GEOSTROPHIC +

Figure 1. Transformation from x to $x - \frac{v_g}{f}$ coordinates.

5-10 km wide, which may themselves form bands. The distribution of the variously orientated mesoscale bands form a reasonably consistent picture which is shown in Figure 2.

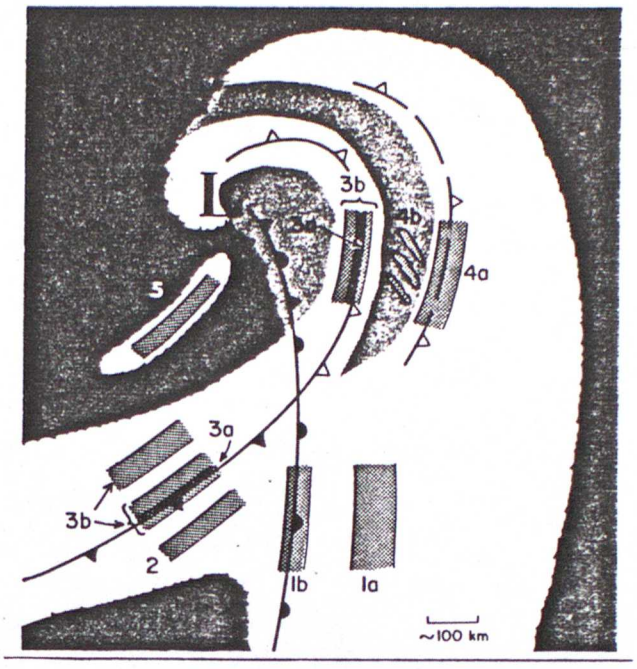

Figure 2. Schematic depiction of the types of mesoscale rainbands (darkly stippled areas) observed in extratropical cyclones. The upper-level cloud shield of the cyclone is shown as white; lower cloud decks are shaded light gray. Type 1: Warm frontal rainbands, of which type 1a occurs ahead of and parallel to the surface warm front, while type 1b coincides with the surface warm front. Type 2: Warm sector rainbands, which occur parallel to and ahead of the surface cold front. Type 3: Cold frontal rainbands, of which type 3a is very narrow and coincides with the cold frontal passage, while type 3b is wider and may straddle the narrow cold frontal rainband or lag behind it. Type 4: The surge rainband, type 4a, coincides with the leading edge of a surge of cold air aloft, ahead of the main cold front in the occluded portion of the cyclone. A field of convection, frequently organized in small rainbands, type 4b, occurs behind the surge rainband. Type 5: Postfrontal rainbands, which occur in the cold air mass to the rear of and parallel to the cold front and usually to the rear of the large cirrus shield associated with the cyclone.

Type 1. Warm frontal rainbands, of which type 1a occur ahead of and parallel to the surface warm front, while 1b coincides with the surface warm front.

Type 2. Warm sector rainbands which occur parallel to and ahead of the surface cold front.

Type 3. Cold frontal rainbands, of which type 3a is very narrow and coincides with the surface cold front, while type 3b is wider and may straddle the narrow cold frontal rainband or lag behind it.

Type 4. The surge rainband, type 4a, coincides with the leading edge of a surge of cold air aloft, ahead of the main cold front in the occluded portion of the cyclone. A field of convection, frequently organized into small rainbands, type 4b occurs behind the surge rainband.

Type 5. Post frontal rainbands, which occur in the cold air mass to the rear of and parallel to the cold front and usually to the rear of the large cirrus shield associated with the cyclone.

Type 5 may sometimes be seen on satellite pictures but all the remaining types are embedded in the frontal cloud canopy and are visible only through precipitation radar. An example is illustrated in Figure 3.

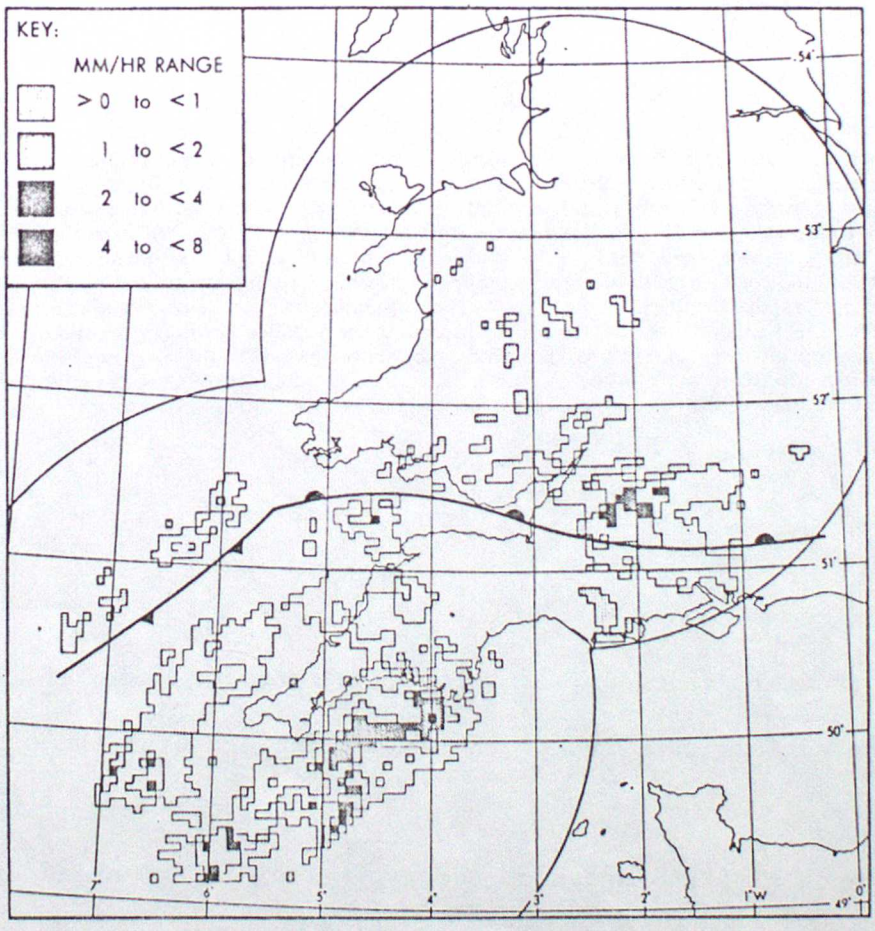

Figure 3. Rainfall distribution in a wave depression showing 3 bands. 2 of type 2 and 1 of type 3b.

3. Type 3a or Narrow Cold Frontal Rainband

This type of band is coincident with the surface cold front and is due to forced ascent as cold air undercuts the warm moist warm-sector air. Figures 4 and 5 illustrate the type of motion and resulting precipitation in a typical cold front.

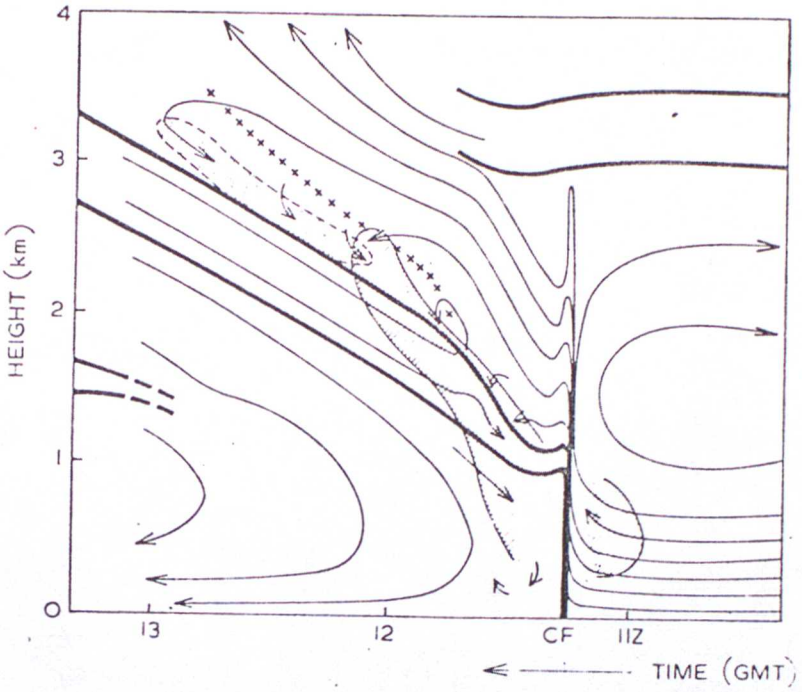

Figure 4 Time-height section showing the transverse circulation in the vicinity of the cold front of 6 February 1969 as it passed over Pershore, derived from Fig. 6. Thin solid lines are streamlines of flow relative to the system. Thick lines denote the boundaries of the frontal zone and other stable layers. Crosses denote the base of the main frontal cloud deck as inferred from the $w = 0$ isotach in Fig. 6 (e). Hatched shading indicates $(\partial u/\partial x) > 20 \times 10^{-5}\ s^{-1}$; stippled shading indicates $|\partial V/\partial z| > 3 \times 10^{-2}\ s^{-1}$.

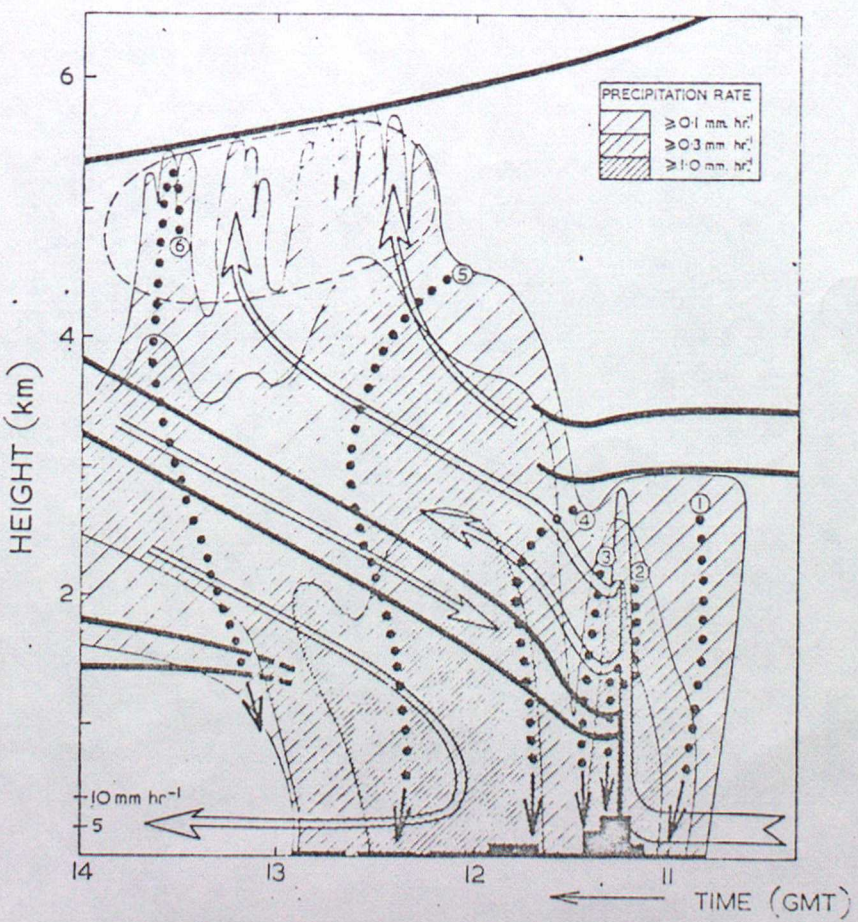

Figure 5 Time-height section showing precipitation intensity in the vicinity of the cold front of 6 February 1969 as it passed over Pershore. The three levels of shading correspond to estimated precipitation rates aloft in excess of 0·1, 0·3 and 1 mm hr⁻¹. Surface rainfall rate at Pershore is indicated along the abscissa. (The most intense precipitation occurred at the SCF; however, because of the presence of hail in this region it is not possible to interpret quantitatively the radar reflectivity in terms of precipitation rate aloft). Solid arrows are streamlines, dotted lines are precipitation trajectories, thick lines denote the boundaries of the frontal zone and other stable layers, and the dashed line delineates the extent of small-scale convection at high levels.

4. Type 4b

As depicted in Figure 1 this type of band usually occurs behind a surge of cold air and the bands are generally embedded within a larger, amorphous region of rain. Similar looking bands are often found embedded within Type 2 and 3a and these have been investigated in detail. They were found to be due to low level longitudinal rolls aligned parallel to the wind and situated in the warm sector. This is illustrated in Figure 6. The bands are associated with the regions of ascent.

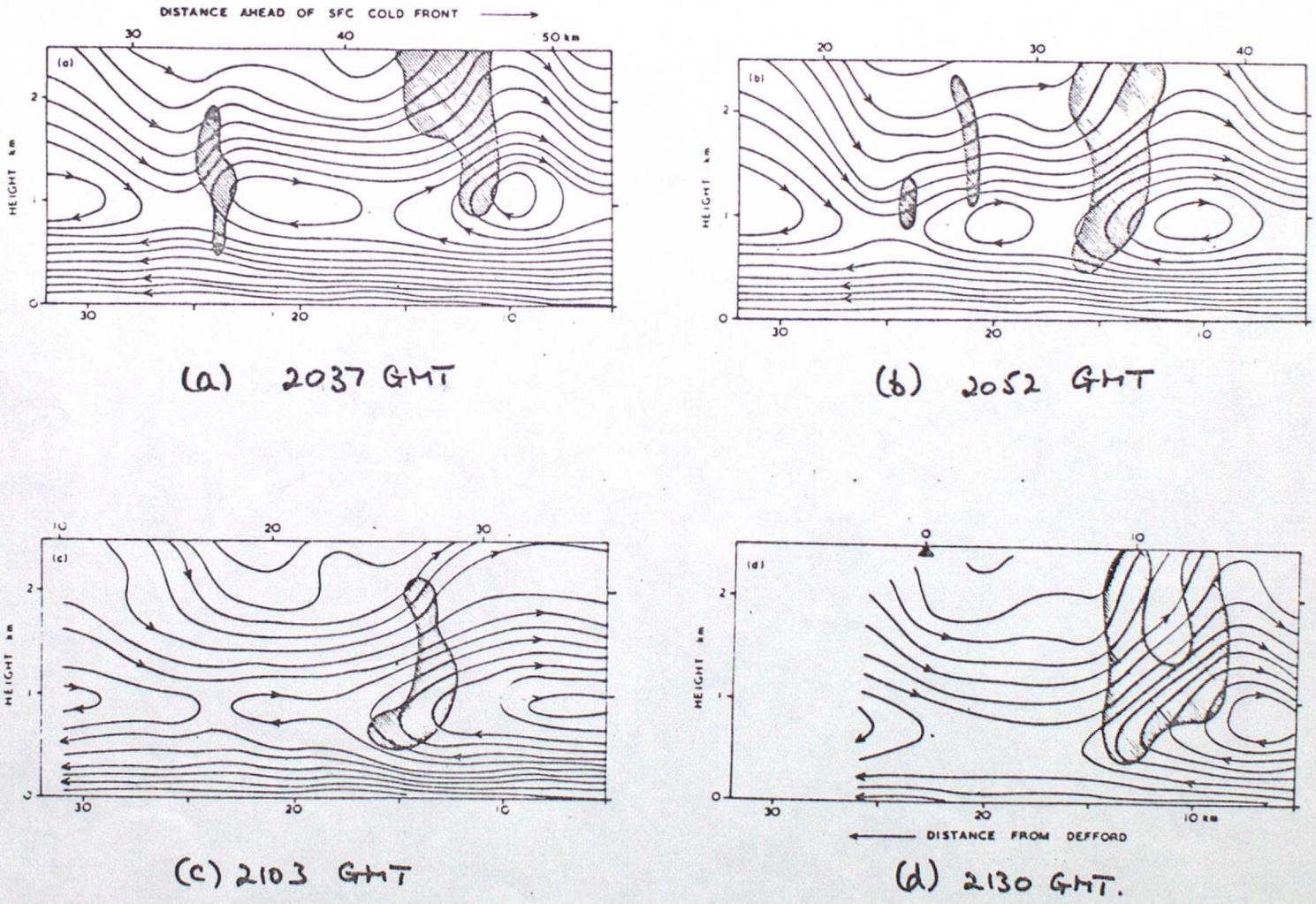

Figure 6. Pattern of airflow within vertical sections (x–z) normal to the rainband at (a) 2037, (b) 2052, (c) 2103 and (d) 2130GMT. Regions where the vertical velocity exceeds 30cm s^{-1} are hatched. The horizontal axes are labelled at the bottom of the diagrams in terms of distance from Defford normal to the rainbands and, at the top of each diagram, in terms of the distance ahead of the approaching surface cold front.

The rolls are clearly induced by frictional effects within the boundary. Although not yet proven, it is possible that bands type 4b have a similar origin, the difference in manifestation being that in the warm sector the rolls enhance a predominantly uniform stratocumulus layer whereas behind the surge rainband (Figure 1) they organize a field of convection.

5. Types 1a, 1b, 2, 3 band 4a

Although occurring at very different positions within the cyclone these types have sufficient similar characteristics to be commonly described. Their width is ~ 50 to 100 km and they are embedded within the frontal flow having little motion relative to the frontal zones with which they are associated. It is usual to envisage them as perturbations within the larger scale frontal dynamics, the perturbations modifying the existing distribution of cloud water rather than generating it.

As already mentioned, their manifestation is by radar observations of rainfall. By flying instrumented aircraft through the bands the increased rainfall can be understood in terms of the microphysical structure of the clouds. Associated with the bands are

1) regions of potential instability at the mid-level of the atmosphere.

2) increased numbers of ice crystals at high levels.

The implication is that within the regions of potential instability convective clouds grow. These "seed" the underlying frontal cloud and create regions of enhanced rainfall. Since the regions of instability tend to be two-dimensional the enchanced rainfall occurs in bands. What is not answered is

1) why do the region of potential instability exist?

and 2) do they cause the mid-level release of convection or are they generated by it?

In either event their significance is now apparent and Figure 7 shows a cross section of wet bulb potential temperature through a frontal zone described in a previous lecture and Figure 8 shows the relative humidity.

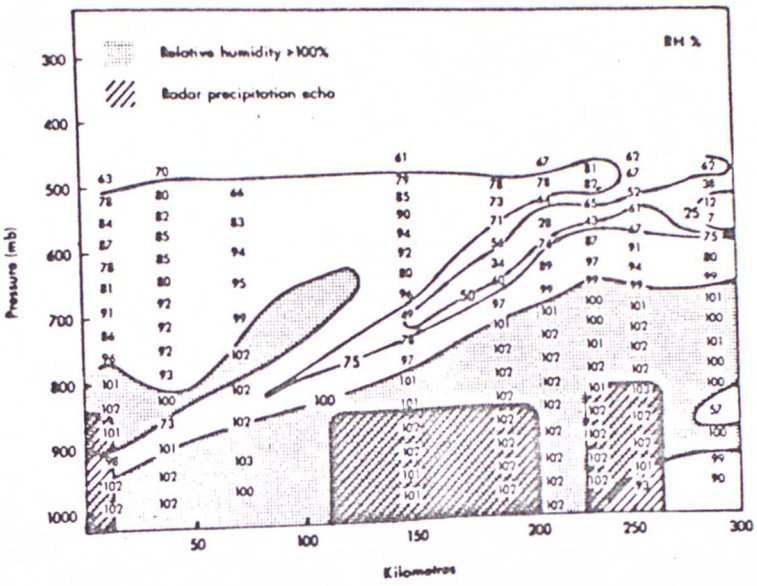

Figure 7. East-West cross section of relative humidity and radar echo.

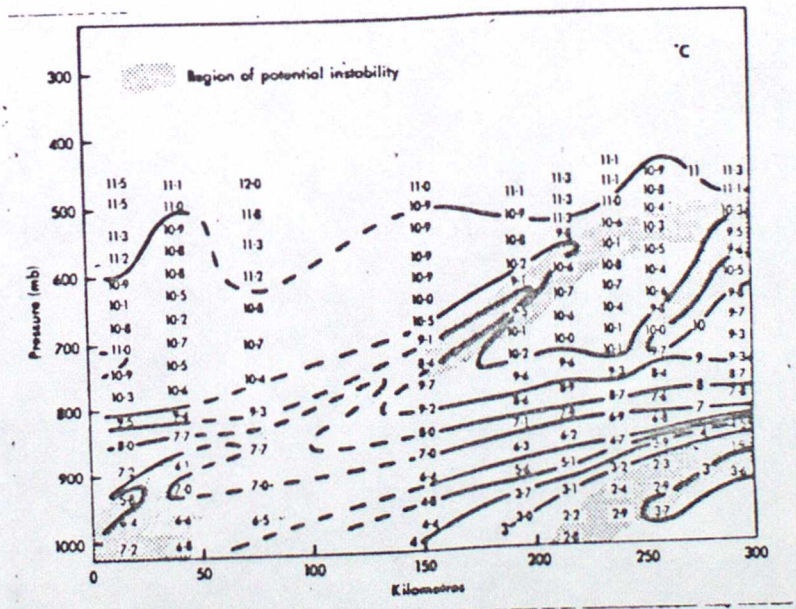

Figure 8. East-West cross section of wet bulb potential temperature.

There are four regions of interest. Two of them (250 km, 600 mb) and (250 km, 950 mb) occur in dry air and the instability is unlikely to be released. The remaining two centred at (260 km, 720 mb) and (50 km, 1000 mb) occur in saturated air and are coincident with bands in the rain. The third and largest region of rain probably results from the larger scale frontal ascent.

6. Type 5

Less is known about this type of convective rainband but the few case studies that have been made indicate that it can take a variety of forms. At one extreme it can have the characteristics of a secondary cold front or trough a few hundred kilometres behind the main front and at the other extreme appears as a loosely linked line of convective clouds.

There is some evidence to suggest that those having frontal characteristics are created by the synoptic scale motion while those of a convective nature are of mesoscale origin and have some similarity to Types 1a, 1b, 2, 3b and 4a. To illustrate this element a case study of some Type 5 bands will be presented.

The synoptic situation is shown in Figure 9 for 1200 GMT on 19 December 1980. The vigorous cyclone situated 300 miles west of Scotland was moving slowly East and had begun to decay. Vigorous convection developed in the cold air behind the cold front especially in the pool of cold air marked C. Individual cumulonimbus clouds reached $\sim$7 km, their growth being assisted by the large scale ascent generated beneath the left exit of the upper tropospheric jet. The crosses mark the ends of the line on which sondes were dropped.

Figure 10 is a diagramatic sketch of the cloud structure seen on the satellite picture taken $2\frac{1}{2}$ hours previously, with the path of the aircraft superimposed. Crosses mark the positions in which the sondes were ejected at a height of 24,000 ft. The additional traverses were made at lower levels to obtain microphysical measurements.

Figure 11 is a schematic representation of the flight plan and cloud structure in a vertical section.

SURFACE ANALYSIS
1000 - 500 MB THICKNESS
500 MB ANALYSIS
250 MB ANALYSIS

Figure 9.

Figure 10. OUTLINE OF CIRRUS CLOUD AND FLIGHT PATH.

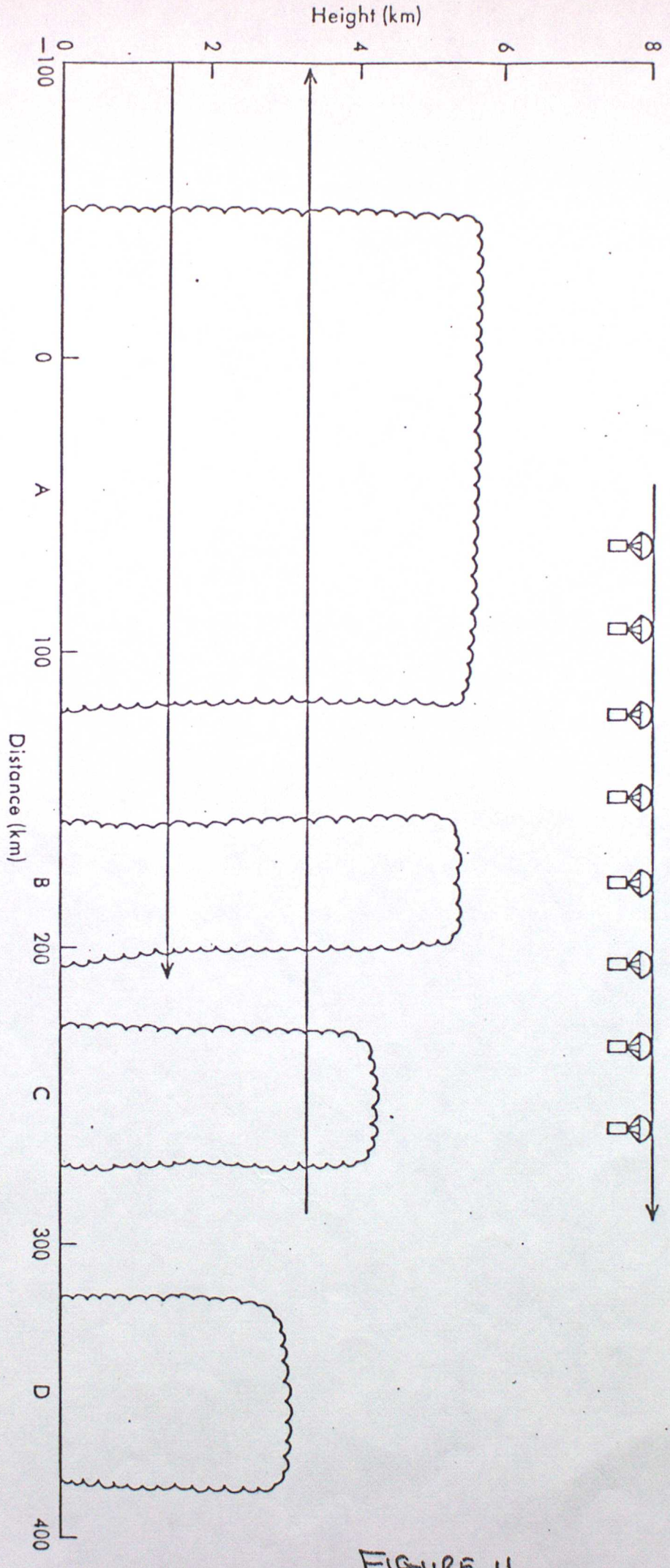

FIGURE 11.

Figure 12 shows the relative humidity measured by the sondes with the regions saturated with respect to water heavily stippled. Three bands were evident at 100, 200 and 275 km corresponding to cloud bands A, B and C respectively. The bands B and C retained their identity reasonably well during the 2½ hours from the satellite picture. The evolution of band A was more difficult to follow partly because the sonde pattern was dropped through a particularly complex region and partly because the lower cloud structure was obscurred by cirrus.

The bands were separated by dry zones which are delineated by the 60% relative humidity contour. The lighter stippled regions delineate air with a relative humidity between water and ice saturation, but whether or not cloud particles were present depends critically upon its recent history.

During their descent the sondes also measured the wind field, from which can be calculated instantaneous streamlines. Figure 13 shows these superimposed onto the humidity field, dashed lines indicat some uncertainty in the data. It is evident that there is descent in dry regions and ascent in cloudy regions.

From the data, of which only a small fraction has been presented, it is possible to construct a typical post cold frontal convective band and this is shown in Figure 14.

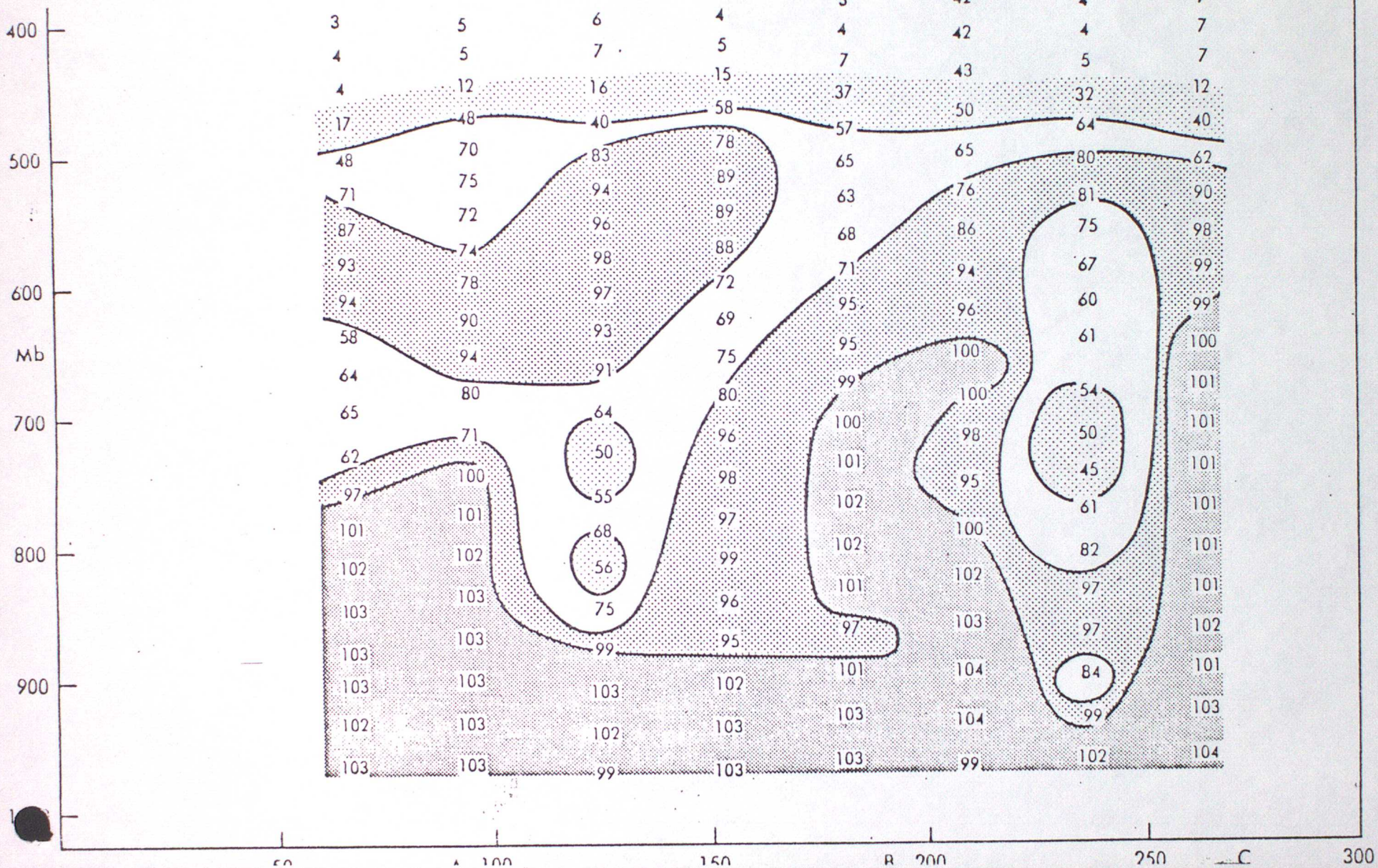

Figure 12. Relative humidity. Heavy stippled indicates saturation w.r.t. water and light stippled saturation w.r.t. ice.

Figure 13. Streamlines superimposed onto the relative humidity field.

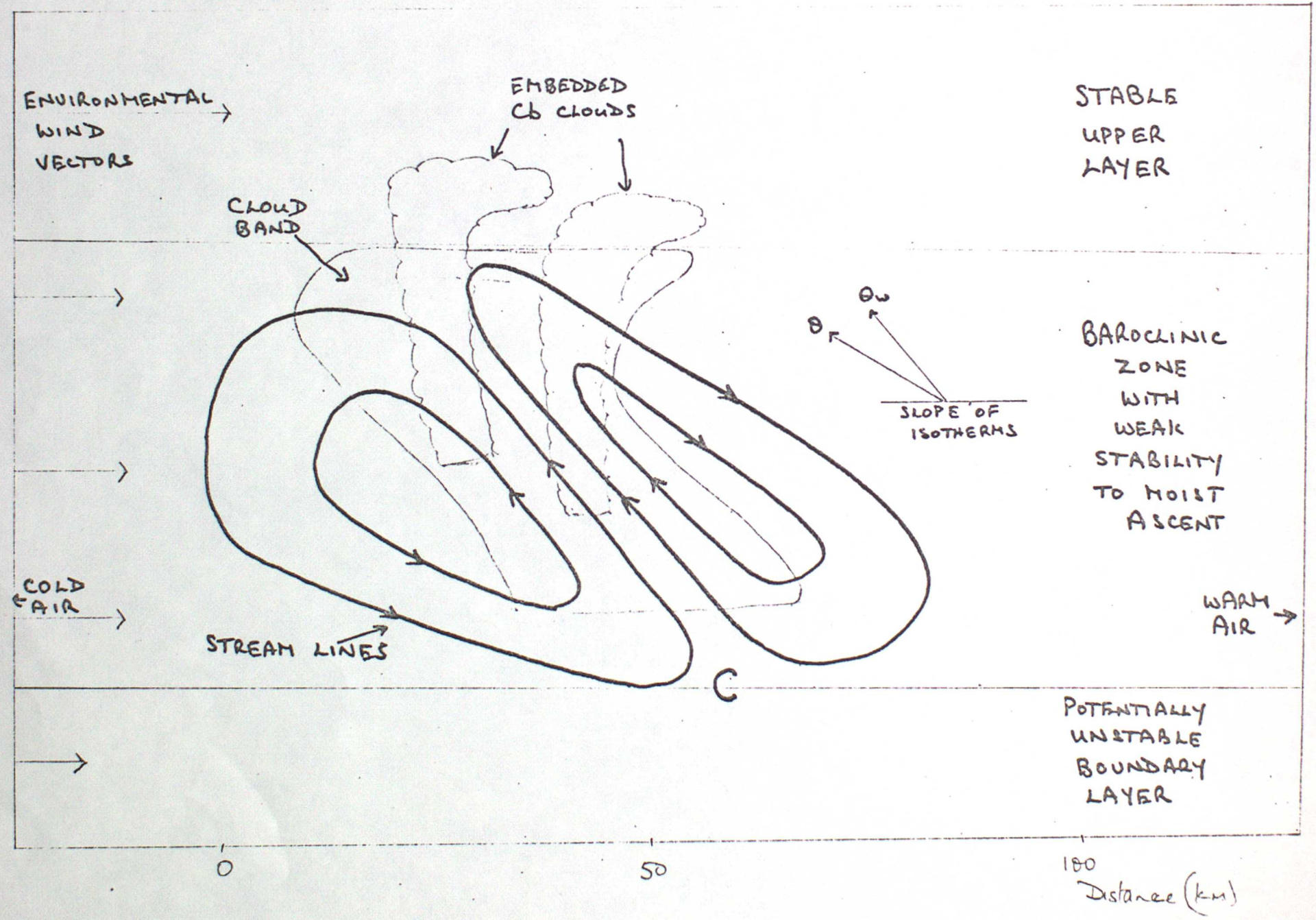

Figure 14. Schematic diagram of a post cold frontal rainband.

1. INTRODUCTION

In the previous lecture the various types of rainbands shown in Figure 1 were discussed.

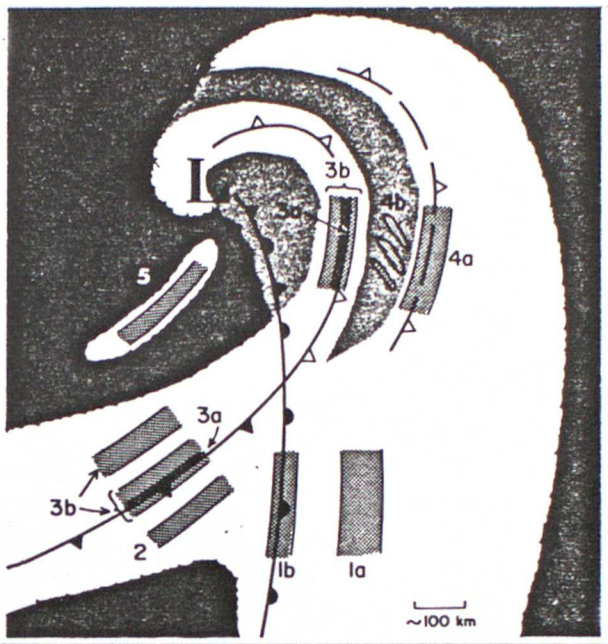

Figure 1. Schematic depiction of the types of mesoscale rainbands (darkly stippled areas) observed in extratropical cyclones. The upper-level cloud shield of the cyclone is shown as white; lower cloud decks are shaded light gray. Type 1: Warm frontal rainbands, of which type 1a occurs ahead of and parallel to the surface warm front, while type 1b coincides with the surface warm front. Type 2: Warm sector rainbands, which occur parallel to and ahead of the surface cold front. Type 3: Cold frontal rainbands, of which type 3a is very narrow and coincides with the cold frontal passage, while type 3b is wider and may straddle the narrow cold frontal rainband or lag behind it. Type 4: The surge rainband, type 4a, coincides with the leading edge of a surge of cold air aloft, ahead of the main cold front in the occluded portion of the cyclone. A field of convection, frequently organized in small rainbands, type 4b, occurs behind the surge rainband. Type 5: Postfrontal rainbands, which occur in the cold air mass to the rear of and parallel to the cold front and usually to the rear of the large cirrus shield associated with the cyclone.

Types 3a (narrow cold frontal) and 4b may be considered as psecial cases and possible explanations for their existance have already been described. Some evidence was presented that types 1a, 1b, 2, 3b and 4a together with some examples of type 5 had certain features in common. Their width was 50–100 km, their lifetime 12–24 hours and the motion fields associated with them extended over a considerable depth, in excess of half the height of the tropopause.

The bands embedded within the frontal canopy have been observed by many research workers (see bibliography). Although there is some disagreement in detail, the common concensus is that the banded rainfall results from regions of potential instability embedded within the frontal zone as shown in Figure 2. Release of the instability occurs through shallow mid-level convection and the additional precipitation embryos thus generated preferentially seed the fairly

uniform frontal cloud. The associated motion fields are frequently in the form of a roll, relative to a set of axes moving with the system, as illustrated in Figure 2.

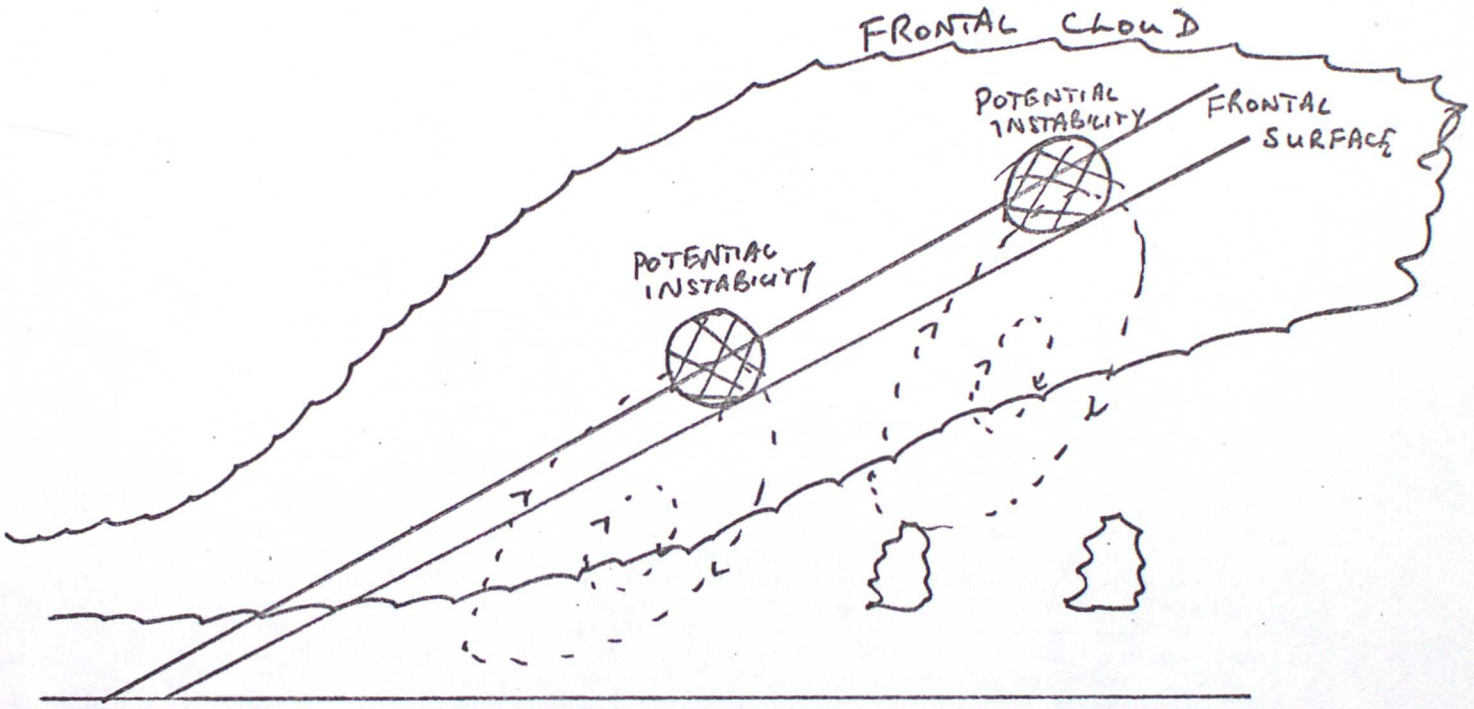

FIGURE 2. SCHEMATIC DIAGRAM OF POSITION OF REGIONS OF POTENTIAL INSTABILITY AND ASSOCIATED FRONT-RELATIVE MOTION

A similar organization is found in some type 5 bands, in particular those that are of mesoscale origin. A schematic represent of one of these bands is shown in Figure 3. It can be seen that the motion fields are similar but instead of the potential instability being confined to a shallow region, it now extends over the whole depth of the tropopause. The ascending and descending motion selectively enhances the growth of convection and the bands appear as an organized region of cumulonimbus clouds. An additional feature of all of these types of bands is that they appear to be embedded within the mean flow, i.e. they have little motion relative to the frontal system with which they are associated.

There are several theories that have been advanced in explanation of frontal rainbands. Since two of the more complete ones are adaptations of symmetric instability this will be described first.

2. Symmetric Instability

Symmetric instability derives its name from the symmetric baroclinic vortex ie the global circular flow round either of the poles of the earth. The word symmetric implied that the motion was independent of (in cylindrical polar co-ordinates). In the present context it is easier to visualise a uniform, 2-dimensional, baroclinic zone. Symmetric instabilities then form as roll perturbation with their axis along the baroclinic zone and the circulation in the plane of baroclinicity.

Symmetric instabilities can occur in a dry atmosphere and in many ways can be considered as part of a hierarchy of instabilities comprising of

a. Convective instability

Particles move almost vertically crossing isotherms. The growth rate ie the Brunt-Vaisala frequency is typically 10-20 minutes and the motion depends primarily on $N^2 = \frac{g}{\theta_0}\frac{\partial\theta}{\partial z}$. The instability can be considered to be 1-D.

b. Symmetric instability

Particles move close to the isotherms but can cross them. The growth rate in form $\sim$ 6-18 hours (strictly $<$ 24 hours) and depends on both N^2, f^2 and S^2 where f is the coriolis parameter and $S^2 = \frac{g}{\theta_0}\frac{\partial\theta}{\partial x}$. The instability is 2-D.

c. Baroclinic instability

Particles move along isotherms. The growth rate is $\sim$ 1-2 days (strictly $>$1 day) and depends primarily on f^2 and the horizontal temperature gradient S^2. The instability is 3-D.

An example of symmetric instability is shown in Figure 4. The lower part shows the isotherms within a uniform baroclinic zone. Although they appear almost vertical due to the axes chosen, in the atmosphere they lie almost horizontal with a slope of $\sim$ 1/75. The scale indicates the interval between

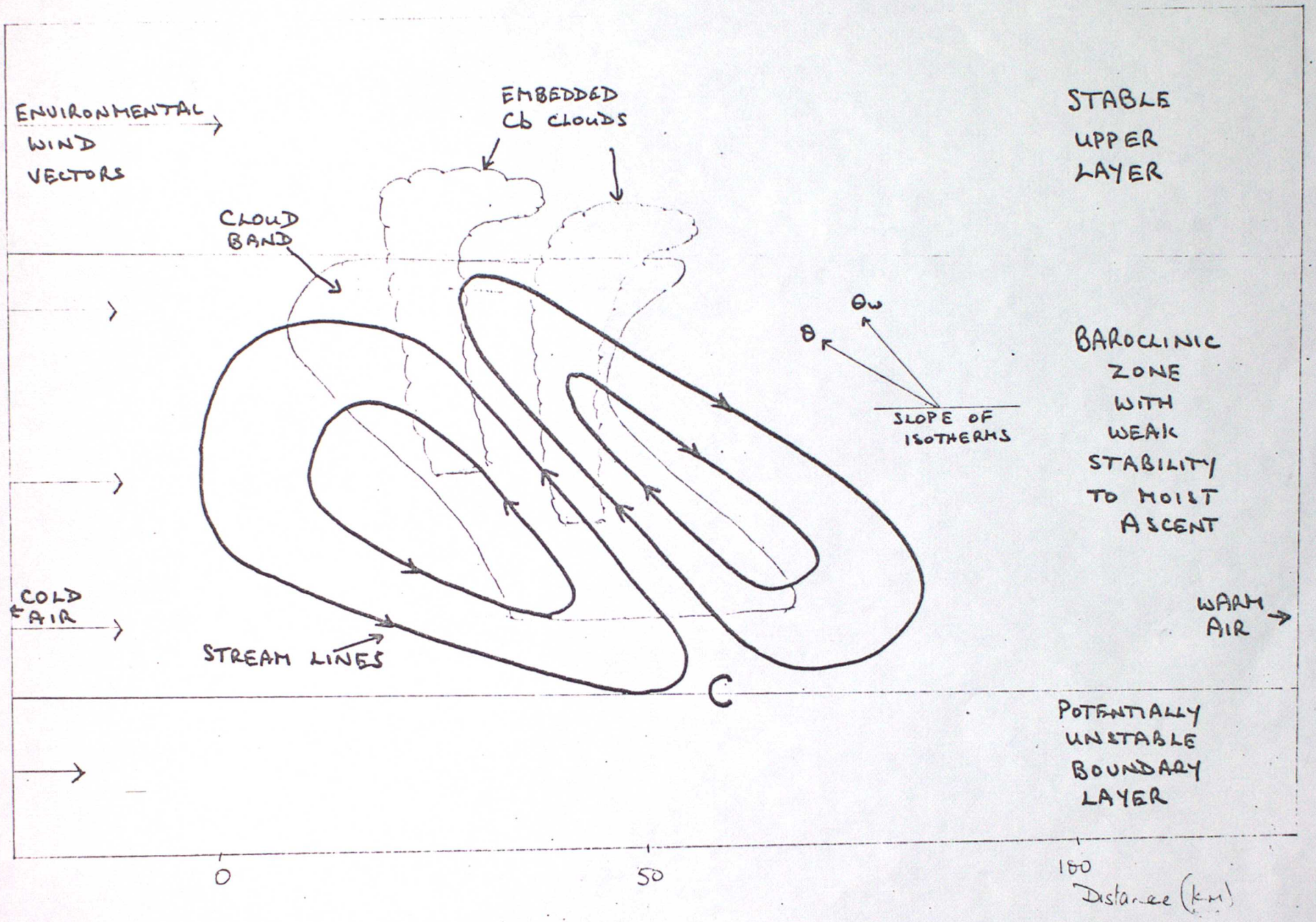

Figure 3. Schematic representation of a Type S rainband.

successive contours. The top part of Figure 4 shows the streamlines of symmetric instability, solid contours indicate clockwise and dashed anti-clockwise motion. Again, due to the axes the rolls appear vertical but in practice have a slope close to that of the isotherms. Typical vertical velocities are $O(10\ cm\ s^{-1})$.

An atmosphere is said to be symmetrically unstable if the Richardson number

$$R_i > 1$$

where $R_i = \frac{N^2F^2}{S^4}$

$N^2 = \frac{g}{\theta_0}\frac{\partial\theta}{\partial z}$ - Brunt-Vaisala

$F^2 = f\left(f + \frac{\partial v}{\partial x}\right)$

$S^2 = \frac{g}{\theta_0}\frac{\partial\theta}{\partial x}\ \left(= f\frac{\partial v}{\partial z}\right)$ Thermal wind.

i.e. the Richardson number is the ratio of the static stability to the vertical wind shear.

In a frontal zone

$\frac{\partial\theta}{\partial z} \sim 6^\circ\ km^{-1}$ $\qquad$ $\frac{\partial\theta}{\partial x} = 40^\circ$ per $100\ km$

$\frac{\partial v}{\partial x} \sim 0.5f$ $\qquad$ $\theta_0 \sim 287$

$N \sim 1.4\times10^{-2}\ s^{-1}$, $F = 1.2\times10^{-4}\ s^{-1}$, $S = 1.2\times10^{-3}\ s^{-1}$

and hence $R_i \sim 1.4$.

In other words, most frontal zones are generally stable to symmetric instabilities.

3. Conditional Symmetric Instability (CSI)

However in a saturated frontal zone there is latent heat release on ascent; parcels of air ascend on θ_w surfaces but descend on θ surfaces. The effect of this is to assist the symmetric instability. The Brunt-Vaisala

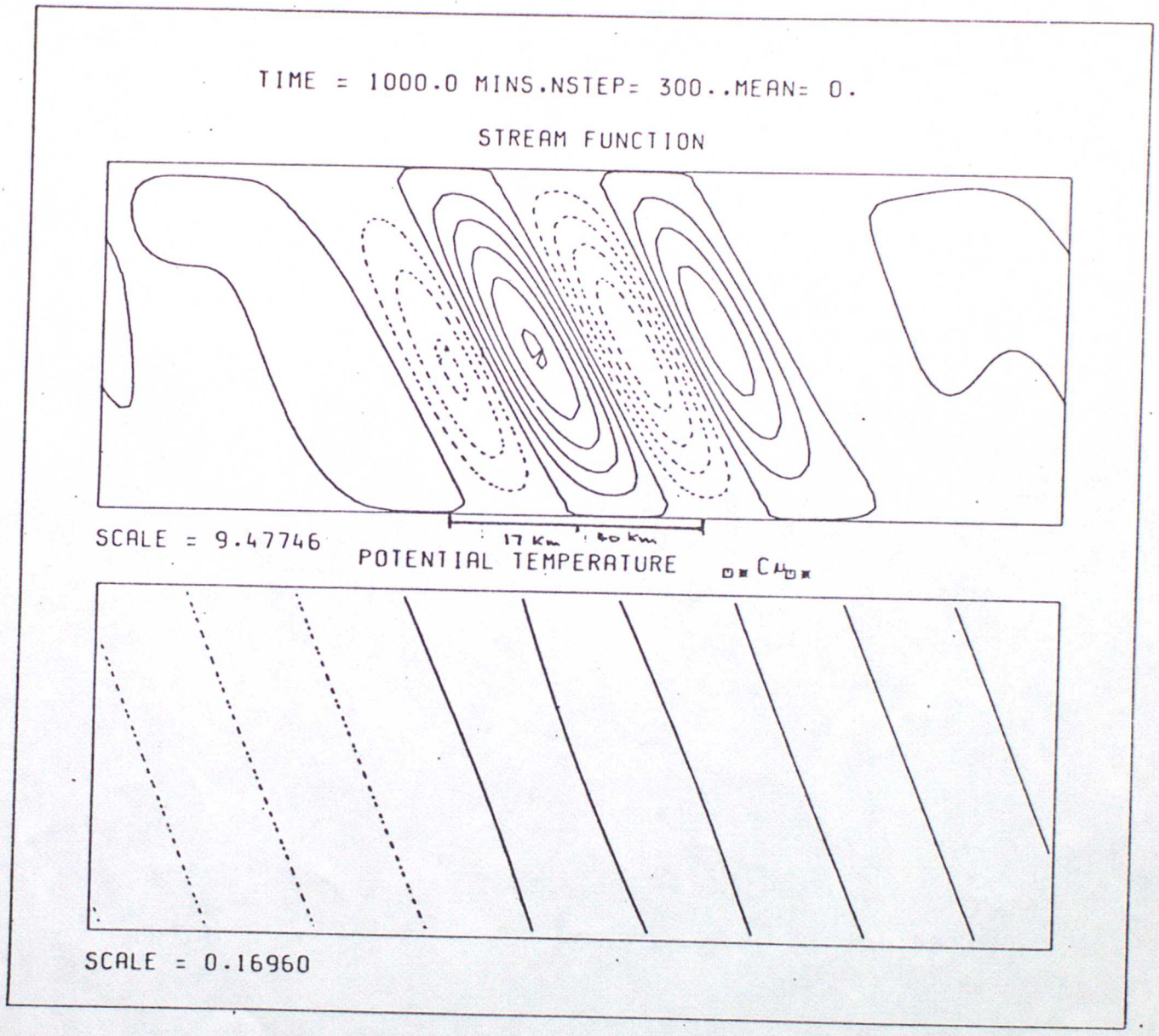

Figure 4 Symmetric Instability.

frequency is modified and the change can be crudely represented by replacing

$$N^2 \text{ by } N_M^2 = \tfrac{1}{2}(N^2 + N_w^2)$$

where $$N_w^2 = \frac{g}{\theta_0}\frac{\partial \theta_w}{\partial z}$$

ie $$N_M = \sqrt{\tfrac{1}{2}}\,\frac{g}{\theta_0}\left(\frac{\partial \theta}{\partial z} + \frac{\partial \theta_w}{\partial z}\right)$$

$$= \sqrt{\frac{g}{\theta_0}\left(\frac{6}{1000} + \frac{1}{1000}\right)}$$

$$\sim 10^{-2}\ s^{-1}$$

giving $$Ri_w \sim 0.7$$

The release of latent heat is sufficient to permit CSI to develop in frontal zones.

A typical example of the growth of CSI is shown in Figure 5.

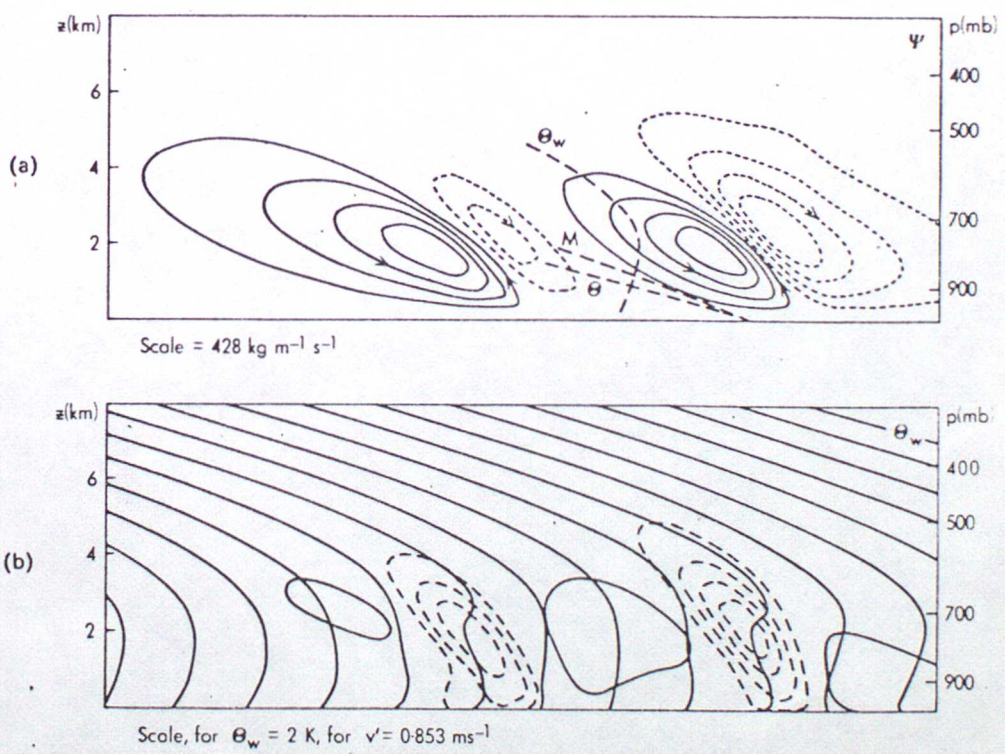

Figure 5 Day ¾ of experiment B. Shown are (a) cross-band streamfunction with initial Θ, Θ_w and M surfaces indicated; and (b) wet bulb potential temperature and wind perturbation along the band. Contour convention as in Fig 6

The upper part of Figure 5 shows the streamlines of two CSI rolls, solid lines anticlockwise and dotted lines clockwise. In SI (Figure 4) the up and downdraughts were parallel and had equal magnitude but in CSI the drive for the instability occurs only on ascent creating a strong and narrow updraught parallel to the θ_w isotherms. The descent is dry and hence stable,

and in consequence has to be forced and is therefore parallel to θ lines and occurs over a more diffuse region.

The lower part of Figure 5 shows the wet bulb potential temperature isotherms. Since there is little water vapour at the top the slope of the surfaces may also be inferred. At the bottom of the atmosphere there is neutral stability to convection and the situation typifies the conditions that may be expected in type 5 bands. Notice how the streamlines (Figure 5a) increase the static stability on descent and decrease if an ascent. (The dashed lines in Figure 5b are of the velocity component along the band).

For comparison the schematic diagram of a type 5 band is shown in Figure 3.

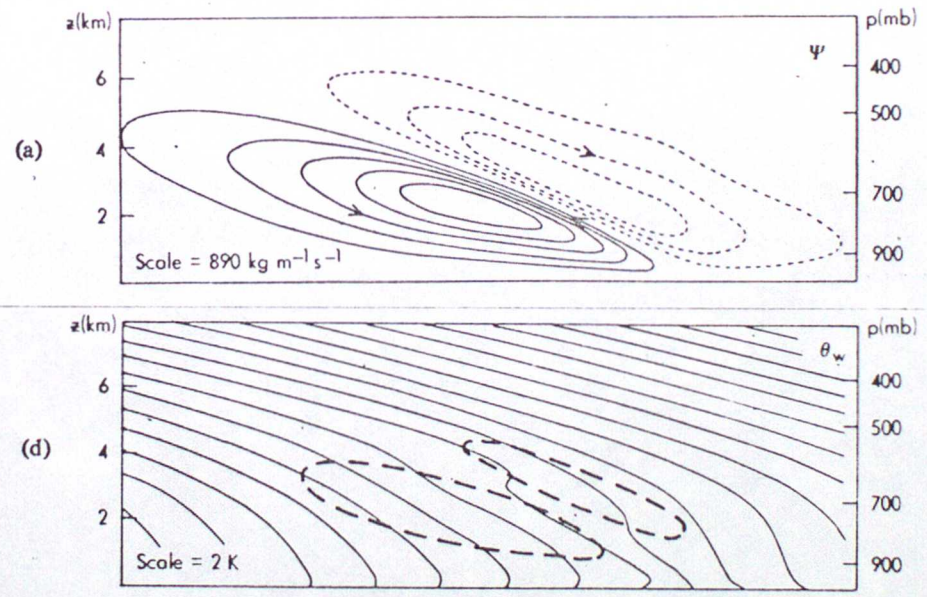

Figure 6 Day 1 of experiment A described in the text. Shown are (a) cross-band streamfunction, , (d) wet bulb potential temperature : .. The contour spacing is shown below each figure. The zero contour is not drawn. Negative contours are dashed. In (b), (c) and (d) the ±3 streamfunction contours are indicated by long dashes. .. Only 700 km of the total 1000 km horizontal domain is shown.

Figure 6 shows the growth of a CSI band in more stable conditions. The same advective properties are apparent but only in a thin mid-level region are the θ_w isotherms overturned producing the small regions of potential instability noted in the study of warm frontal rainbands.

To conclude the section on CSI the possibility of forecasting rainbands is considered. Whether or not CSI is present depends only on the magnitude of N^2, F^2 and S^4 within the frontal zone, ie on scales of 200 or 300 km. It is therefore possible to evaluate the growth rate of CSI from the rectangle forecase model. Figure 7 shows an example. The region of high growth rate to the SW of England, positioned at the tip of the cold frontal wave, coincides well with the bands observed on the Camborne radar; those parallel with the cold front (2 x type 2 and 1 x type 3b). The region of rain over central southern England is on the edge of the region of expected growth but is too small for any assessment of bandedness.

4. Symmetric CISK in a baroclinic flow

An alternative mechanism (Emanuel 1981) considers a different way in which symmetric instabilities may be modified so that they become unstable in frontal zones. The mechanism is called symmetric baroclinic wave-CISK. It differs from CSI in that wave CISK extracts potential energy from convective processes whereas CSI is enhanced by the latent heat release. Symmetric baroclinic wave CISK can therefore only grow in a region already convectively unstable and is therefore applicable only to band occurring on or behind the cold front, types 3b, 5 and possibly 3a.

Symmetric baroclinic wave CISK appears as a propagating band of cumulonimbus clouds. The clouds derive their energy from the potential energy of the atmosphere and their organization from the symmetric instability, essentially the characteristic of a squall line.

There is one drawback in this model of a frontal rainband; the bands propagate relative to the mean flow, whereas observations of rainbands suggest t hat the bands are embedded within the flow. However sufficient measurements

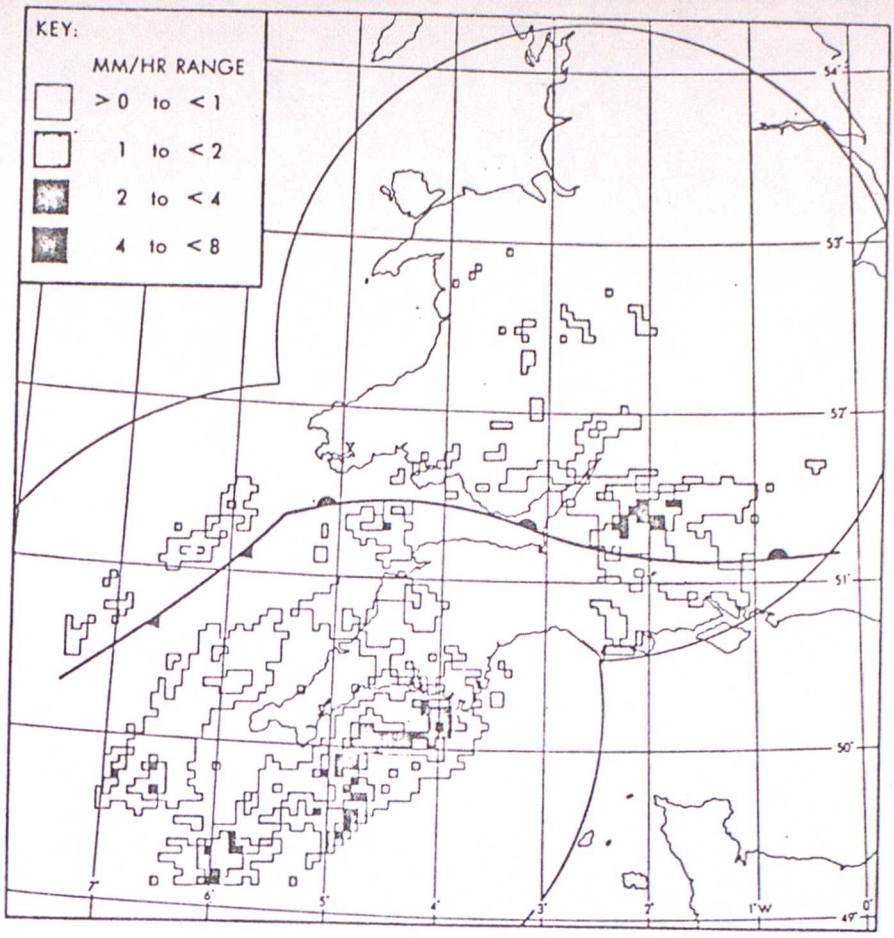

(a)

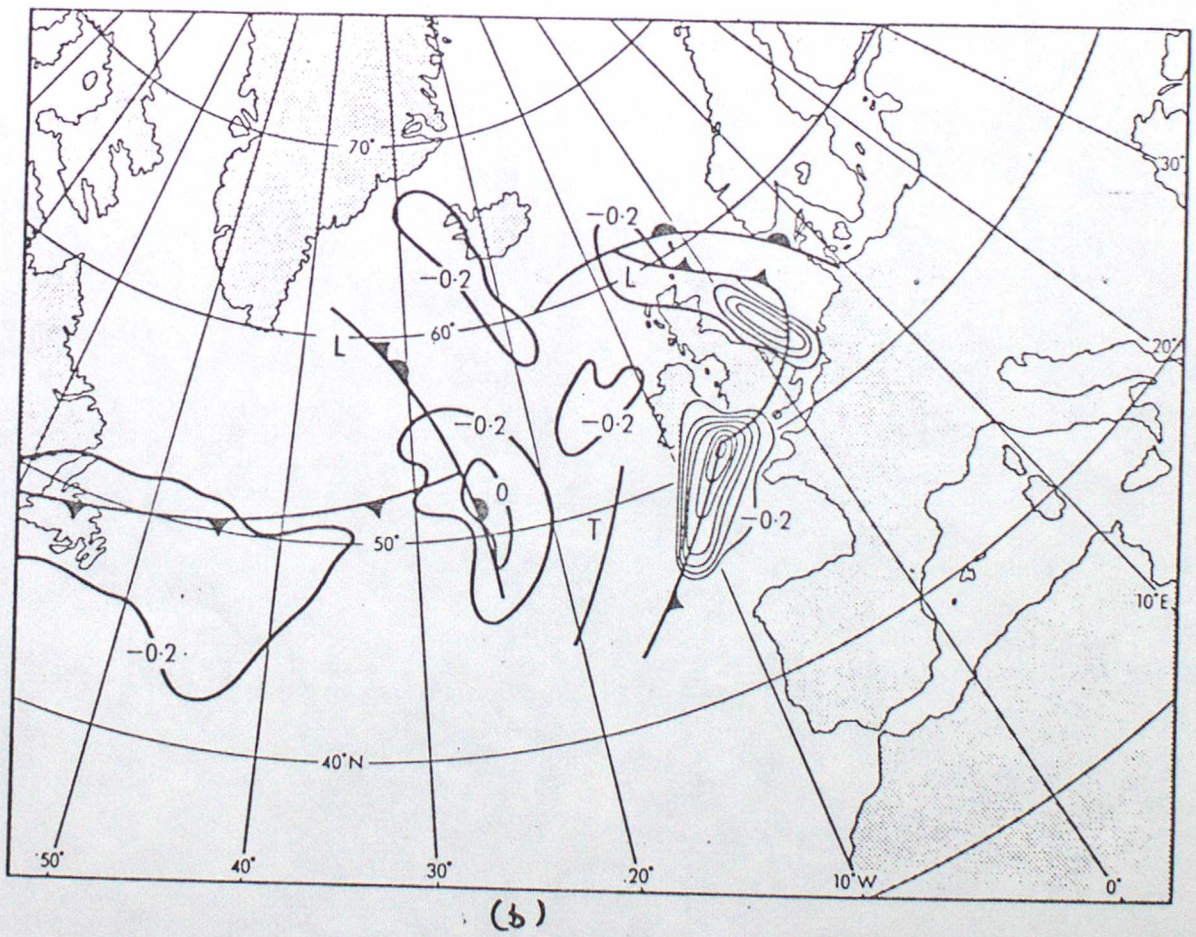

(b)

Figure 7. Comparsion between observations of rainbands (a) and predictions of the Rectangle forecast Model (b). The region of interest is over S. W. England.

have not yet been made for a complete evaluation of the theory and it provides a good description of many of the features of those rainbands that result predominantly from convective processes.

5. Rainbands as a line of multicellular storms

If the band, for example type 5, appear to be an organization of cumulonimbus clouds then it may be generated by multicellular clouds. In each cloud a downdraught is created and maintained by precipitation forcing (evaporation and drag) which, on encountering the ground, spreads out as a cold density current. A gust front forms on the boundary of the cold air, being strongest along the direction of the cloud relative inflow, where new convection is generated. Some recent work (Thorpe et al 1980) suggests that this process may be enchanced if the individual clouds are aligned perpendicular to the low level inflow, thus providing the necessary organization.

6. Rainbands as a manifestation of ducted internal gravity waves

Lindzen and Tung (1976) considered rainbands to be the physical manifestation of ducted mesoscale gravity waves. Conditions suitable for the propagation of such waves can occur within frontal zones as shown in Figure 8, which, on the left hand side, depicts the typical environmental conditions found associated with mesoscale rainbands. Region I refers to the region below the frontal surface, II to the thermodynamically uniform warm air above the front, and III to the regions of mid-tropospheric convective instability (already discussed). The factors that allow the stable moist air to act as a duct for gravity waves (right hand side of Figure 8) are:

a. a stable boundary layer to prevent interaction with the ground.

b. a convectively unstable layer above, to act as a reflector. (A stable or neutral layer is insufficient).

c. a flow speed, which, at some level, equals or comes close to that of the ducted mode (steering level).

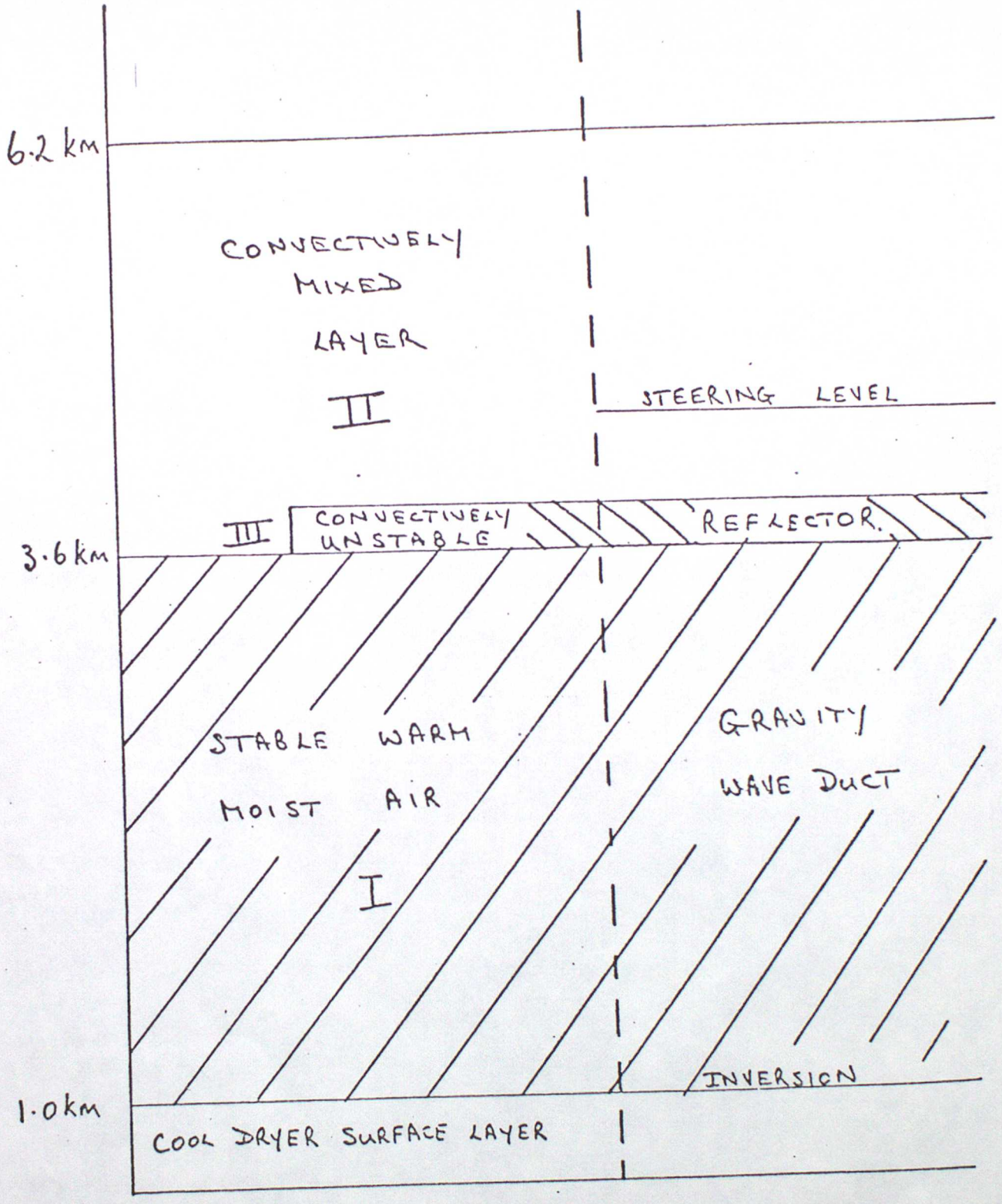

Figure 8. Conditions suitable for the propogation of ducted gravity waves. Lindzen & Tung (1976).

The implication of c_s is that the gravity waves move slowly relative to the frontal system. This is in accord with observations that warm frontal, mesoscale rainbands often travel slightly faster than the associated frontal system (Browning and Harrold 1969).

However the theory does not indicate the wavelength of the bands although calculations relating the speed of propagation to the depth of the layer suggests scales between 10 and 100 km which covers the range observed. Its other major weakness is that it gives no explanation for the (unexpected) existance of a mid-tropospheric unstable layer.

References

Bennetts D A and Hoskins B J 1979 Conditional symmetric instability - a possible explanation for frontal rainbands. Quart J R Met Soc 105 pp 945-962.

Bennetts D A, Lewis A F and Ryder P 1982

Bennetts D A and Rawlins F 1981 Parametrization of the ice-phase in a model of mid-latitude cumulonimbus convection and its influence on the simulation of cloud development. Quart J R Met Soc 107 pp 477-502.

Browning K A and Mason B J 1980 Air motion and precipitation growth in frontal systems. Met Office Radar Research Laboratory Report No 19.

Cunningham R M 1978 Analysis of particle spectral data from optical array (PMS) 1D and 2D sensors. Fourth symposium on meteorological observations and instruments April 10-14 1978 Denver Colorado.

Emanuel K A 1981 Inertial Instability and Mesoscale Convective Systems: Part II: Symmetric CISK in a baroclinic flow. Submitted to J Atmos Sci.

Fletcher N H 1962 The physics of rainclouds. Cambridge University Press.

Hallett J and Mossop S C 1974 Production of secondary ice particles during the riming process. Nature 249 pp 26-28.

Houze R A, Hobbs P V, Biswas K R and Davis W M 1976 Mesoscale rainbands in extra tropical cyclones. Mon Wea Rev 104 pp 868-878.

Matejka T J, Houze R A and Hobbs P V 1980 Microphysics and dynamics of clouds associated with mesoscale rainbands in extratropical cyclones. Quart J R Met Soc 106 pp 29-56.

Miller M J and Betts A K 1977 Travelling convective storms over Venuzuela. Mon Wea Rev 105 pp 833-848.

Moncrieff M W 1981 A theory of organized steady convection and its transport properties. Quart J R Met Soc 109 pp 29-50.

Newton C W 1950 Structure and mechanism of a prefrontal squall line. J Met 7 pp 210-222.

Nichols S 1978 Measurements of turbulence by an instrumented aircraft in a convective atmospheric boundary layer over the sea. Quart J R Met Soc 104 pp 653-678.

Ogura Y and Liou M T 1980 The structure of a mid-latitude squall line: A case study. J Atmos Sci 37 pp 553-567.

Paltridge G W and Platt C M R 1981 Aircraft measurements of solar and infra-red radiation and the microphysics of cirrus cloud. Quart J R Met Soc 107 pp 367-380.

Raymond D J 1975 A model for predicting the movement of continuously propogating convective storms. J Atmos Sci 32 pp 1308-1317.

Roach W T and Hardman M E 1975 Mesoscale air motions derived from wind finding dropsonde data: the warm front and rainbands of 18 January 1971. Quart J R Met Soc 107 pp 437-462.

Roach W T and Slingo A 1979 A high resolution infra-red radiation transfer scheme to study the interaction of radiation with cloud. Quart J R Met Soc 105 pp 603-614.

Thorpe A J, Miller M J and Moncrieff M W 1980 Dynamical models of two dimensional down-draughts. Quart J R Met Soc 106 pp 463-484.

Varley D J 1980 Microphysical properties of a large scale cloud system 1-3 March 1978. AFGL TR-80-0002. Environmental Research Papers No 690.